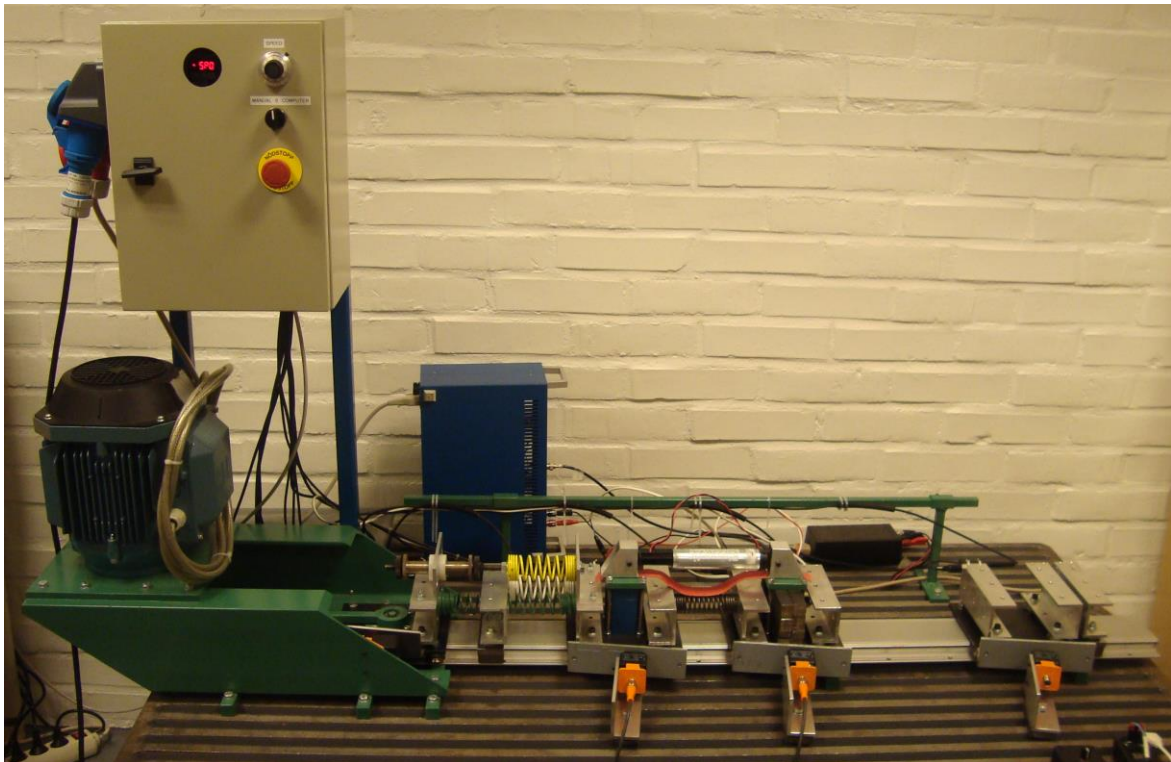# CHALMERS

Semi-Active Vibration Dynamics Control of Multi-Cart Systems Using a Magnetorheological Damper

Master's Thesis in the International Master's programme Applied Mechanics

GEOFFREY GELDHOF

Department of Applied Mechanics
Division of Dynamics
CHALMERS UNIVERSITY OF TECHNOLOGY
Göteborg, Sweden 2013
Master's thesis 2013:21

MASTER'S THESIS IN INTERNATIONAL MASTER'S PROGRAMME APPLIED
MECHANICS

Semi-Active Vibration Dynamics Control of Multi-Cart Systems Using a Magnetorheological Damper

GEOFFREY GELDHOF

Department of Applied Mechanics
Division of Dynamics
CHALMERS UNIVERSITY OF TECHNOLOGY

Göteborg, Sweden 2013

Semi-Active Vibration Dynamics Control of Multi-Cart Systems Using a
Magnetorheological Damper
GEOFFREY GELDHOF

Semi-Active Vibration Dynamics Control of Multi-Cart Systems Using a Magnetorheological Damper
Master's Thesis in the *International Master's programme Applied Mechanics*
GEOFFREY GELDHOF

Department of Applied Mechanics
Division of Dynamics
Chalmers University of Technology

ABSTRACT

Application of Magneto-Rheological (MR) dampers in semi-active vibration dynamics control of a multi-cart system is studied. The dynamics and vibration behaviour of a two cart system is investigated mathematically and an experimental test-rig is employed to verify the model, experimentally. The Bouc-Wen model is utilized to represent the mathematical behaviour of MR damper. Different types of semi-active control strategies as well as passive vibration control technique are implemented in MATLAB and LabView Compaq-RIO. In the passive case, the damping coefficient remains constant during the operation. While in semi-active control strategy, the main idea is to change (in real time) the passive components characteristics to improve the damping performance. Semi-active control technique can be used for vibration control and energy dissipation purposes in different dynamical systems to adjust the damping components and improve the performance while consume a small amount of energy. In this regard, different semi-active control techniques including Skyhook, Groundhook and so on are explored and compared mathematically and experimentally. In each particular case, the root mean square (RMS) values of the first and second cart displacement, velocity and acceleration levels are determined and compared. Finally, the results have shown significant improvement in semi-active control strategies, up to 20%, in comparison with the corresponding optimized passive case.

Key words: Semi-Active Control, Multi-Cart Systems, MR Damper, Vibration Isolation

Preface

The present thesis is carried out at the Division of Dynamics, Applied Mechanics Department, Chalmers University of Technology as a final work to graduate from the Machine Design and Production Engineering Department, University of Mons.

At first, I am truly indebted and thankful to Professor Viktor Berbyuk, Head of the Mechanical Systems research group and co-director of the Vibrations and Smart Structures Lab, for his support, guidance and encouragement.

I am also grateful to my supervisor Mr Seyed Milad Mousavi Bideleh, Ph. D. student at the Division of Dynamics, for his dedication, advice and especially for his help during the writing of the mathematical model of the studied system in MATLAB.

Then, I would like to express my sincere gratitude to Thomas Nygårds who took on his free time to come to Chalmers for helping me when I was working on LabView.

I would like to thank Professor Enrico Filippi, Head of Machine Design and Production Engineering Department, University of Mons, and Pierre Dehombreux, Vice-Rector for International Relations, University of Mons, without whom, this Erasmus exchange would not have occurred.

Finally, all friends that I met during my exchange experience in Sweden cannot be forgotten for their good mood and their support. They were a great source of energy in all the time of my work.

Contents

List of Figures

List of Tables

Notations

Roman upper case letters

A	State (system) matrix
B	Input matrix
B_{MR}	Input matrix from MR damper
C	Damping matrix
F	Force developed by the MR damper
F_{sa}	Semi-active damping force
F_{sky}	Ideal damping force in Skyhook control
H	Magnetic field
I	Damper input current
I_{cont}	Damper input current in continuous control technique
I_{on}	Damper input current when the damper should be in service
I_{off}	Damper input current when the damper should be desactivated
K	Stiffness matrix
M	Mass matrix
R_a	Additional resistance
R_i	Intern resistance of the MR damper
R_{tot}	Total resistance of the circuit
V	Voltage of the electric source

Roman lower case letters

a	Amplitude of the excitation
c	Damping coefficient between the cart and the track
c_0	Damping coefficient of the MR damper model
c_{sa}	Damping coefficient of the semi-active control
c_{sky}	Ideal damping coefficient of the Skyhook control
f	Frequency of the excitation
k_0	Stiffness coefficient of the MR damper model
$k, k_1 k_2, k_3$	Stiffness of the test rig springs
l	Elongation of the spring
l_0	Initial elongation of the spring
m_1	Mass of the unsprung cart
m_2	Mass of the sprung cart
n	Shape parameter of the damping force hysteresis loop
t	Time
u	Base excitation
x	Displacement
$\dot{x}$	Velocity
x_0	Initial displacement
x_1	Displacement of the unsprung mass
x_{12}	Relative displacement between the unsprung and the sprung mass
x_2	Displacement of the sprung mass
x_{21}	Relative displacement between the sprung and the unsprung mass
$\dot{x}_1$	Velocity of the unsprung mass
$\dot{x}_{12}$	Relative velocity between the unsprung and the sprung mass
$\dot{x}_2$	Velocity of the sprung mass

$\dot{x}_{21}$ Relative velocity between the sprung and the unsprung mass

z Evolutionary variable of the MR damper model

z_1, z_2, z_3, z_4 New coordinates in the mathematical model

Greek letters

α Model funcional parameter

β Shape parameter of the damping force hysteresis loop

γ Shape parameter of the damping force hysteresis loop

δ Shape parameter of the damping force hysteresis loop

Abbreviation

FPGA   Field Programmable Gate Arrays

MR   Magnetorheological

PSD   Power Spectral Density

RMS   Root Mean Square

1 Introduction

1.1 Context

The expectations of today's society are becoming more and more draconian over time especially in terms of comfort and safety and vehicle suspension systems are no exception to this rule. By example, the automobile industry has two specific purposes in this field. On one hand, it is always desired to limit the oscillatory movements of the vehicle. This means that the ride comfort of the passengers is improved and on the other hand, within the frame of safety, it inhibits the rebound of the wheels on the road obstacles and maintains them in contact with the ground [Félix-Herrán, 2010]. Another example is the washing machine; indeed, the spinning process is a source of undesired vibrations and of noise. In this case also, a suspension system is used to decrease this discomfort. [Nygårds, 2011][Nygårds-Berbyuk, 2012]

Conventional suspension systems (called passive) are very popular because of the low price, maintenance cost and relatively simple mechanical design. However, even optimized version of such components have saturated in terms of the performance. Indeed, once passive components are designed, a trade-off has to be found between ride comfort and road holding which cannot be changed during the operation and with respect to different operational scenarios. In addition, passive components usually respond to the road excitations on a narrow range of frequencies [Félix-Herrán, 2010] and [Sleiman, 2010].

To meet the growing needs and requirements in terms of safety and ride comfort, several alternatives have been emerged. Such solutions are usually called controllable suspensions because they give the possibility to modify and adapt the damping force in real-time w.r.t the input scenario. It is common to divide such strategies into two general categories: active and semi-active suspensions [Félix-Herrán, 2010].

This work is dedicated to the semi-active solution, because this type of suspension using a magneto-rheological (MR) damper offers both high performance and low power consumption. This technology uses MR fluids that its behaviour is subject to change under the presence of a magnetic field. Therefore, the damping coefficient is adjustable for optimizing the real-time behaviour over a wide excitation frequency range [Sleiman, 2010].

1.2 Purpose

The purpose of this master thesis is to implement the mathematical model of a two cart experimental test-rig using the Bouc-Wen model for the representation of the MR damper force. This computer code (written in MATLAB), is demonstrate the benefits, in terms of vibration reduction, of the semi-active control strategies compared to the passive one A LabView code on the other hand, is implemented and used in the experimental test-rig to experimentally verify the results obtained through the mathematical model. So, different types of semi-active controls are implemented in mathematical and experimental models. First, the passive control is studied, which means that the damping coefficient remains constant during the operation. Then, the semi-active control is applied to the system. The main idea of such control algorithms is to change (in real time) the characteristics of passive devices for energy dissipation and this change usually requires only minimal source of energy. When it comes to the semi-active control, different algorithms exist in the literature. The most common one

is the Sky-hook control, which is considered as the main strategy in this research. After that more semi-active algorithms are compared in order to determine is the most efficient one. The results of the MATLAB code are compared with the corresponding results in LabView 2012 in order to check the applicability and reliability of the obtained results.

1.3 Outline of the report

This report is divided in eight chapters.

The general background and outlines of the work conducted in this Master thesis are described in the first two chapters. The first part of Chapter 2 is dedicated to an overview of MR dampers. While, different types of control strategies including passive, active and semi-active are discussed in the second part. Finally, the semi-active algorithms that will be used in this work are introduced in the last part of this section.

The third chapter presents the test rig that is used in this work. The multi-cart system can be assimilated to a quarter-car model set horizontally. Finally, the particular (MR) damper used in this study is introduced.

Chapter 4 is devoted to the mathematical model of the multi-cart system. It means that first the dynamic equations of this 2-DOF model are written and the corresponding parameters are determined. Then, the solution procedure using MATLAB ODE45 function for the described modelling is explained. Finally, the results and analysis are presented.

Chapter 5 of this thesis deals with the experimental part. This chapter first presents the data acquisition and data processing equipment. Then, describes the construction of the LabView code. After that, the experimental results and verification of the described stages are given. At the end, a comparison between the simulation and the experiments is made.

The purpose of Chapter 6 is to summarize the work that is done for this Master thesis. In addition, the results of testing will be discussed with respect to the research objectives set. The chapter ends with recommendations for future work in the field of semi-active vibration dynamics control.

Chapter 7 is dedicated to the references.

The last chapter of this paper contains the appendixes. Appendix A describes the three common MR fluid operational modes: valve, shear, and squeeze modes. Appendix B presents an analyse of the different models for the modelling of the force exerted by a MR damper. Finally, Appendix C makes a summary of four technologies that are generally used to design the MR dampers.

2 Background

In this chapter, the general background and outlines of the work conducted in this Master thesis are described. The first part of this chapter is dedicated to an overview of MR dampers. While, different types of control strategies including passive, active and semi-active are discussed in the second part. Finally, the semi-active algorithms that will be used in this work are introduced in the last part of this section.

2.1 Magnetorheological dampers

The magnetorheological (MR) dampers are filled with a special amount of (MR) fluid. Once electrical current passes through the electric coil inside of the MR damper, the viscosity of MR fluid and as a result the damping coefficient changes. In the first part of this chapter, MR fluids and their particular properties will be introduced. Afterwards, the MR damper structure and its application in vibration control strategies will be discussed.

2.1.1 Magnetorheological fluids

Magnetorheological fluids are kind of colloidal suspension. In fact, they are usually a mixture of two materials which one is dispersed in the other one (but not chemically bounded to it) at a microscopic level. Based on [Hadadian, 2011] and [Sleiman, 2010], a summary on the MR fluids is given here. In the studied cases there are ferromagnetic particles, typically in the order of 1 to 10 μm in diameter, that are dispersed in a carrier more or less viscous liquid such as mineral or synthetic oil or simply water. Typically, these particles are pure iron and are present at a mass fraction of 80% to 85% in the fluid (or a volume concentration between 20% and 40%). It is necessary to add stabilizers and other additives to the fluid to maintain with certain homogeneity and avoid particle sedimentation.

In the absence of a magnetic field, those fluids exhibit a Newtonian-like behaviour. But when a magnetic field is applied, the iron particles are organized in the form of long chains of spherical magnetic particles (Figure 2-1). This will cause a sudden and significant change in the rheological behaviour of (MR) fluid which is mainly manifested as an increase in the dynamic yield stress or the apparent viscosity of the fluid. In other words, it passes from a liquid state to a semi-solid state.

(a)

(b)
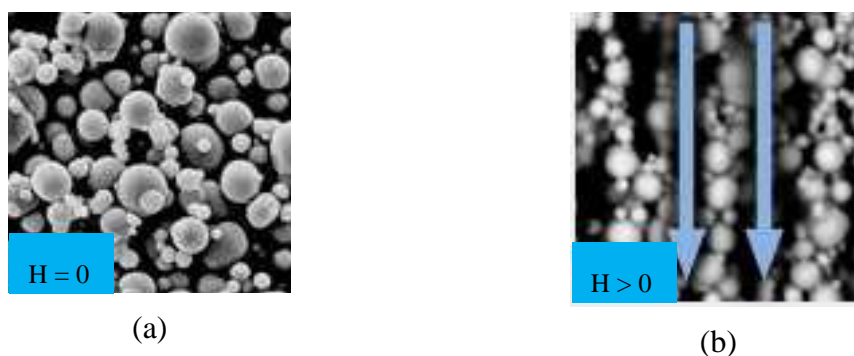
Figure 2-1: Electron microscope image of iron particles MR fluid without a magnetic field (a) and with a magnetic field (b) [BASF 2009]

Figure 2-2 illustrates the organization of particles in the presence of a magnetic field. The organizing mechanism can be explained by the following steps [Lozada, 2007]:

1. In the absence of magnetic field the particles are homogeneously distributed in the carrier liquid.

2. When a magnetic field is applied, it causes the magnetization of the particles which induce a magnetic moment in the same direction as the magnetic field lines.

3. Magnetic particles behave as magnetic dipoles which undergo magnetic interaction forces.

4. Chains are formed following the field lines. This organization corresponds to the minimum energy state.

5. When the field is removed, thermal agitation and the Brownian motion of particles break aggregates and bring the fluid into the initial state. The effect of the afterglow is negligible.
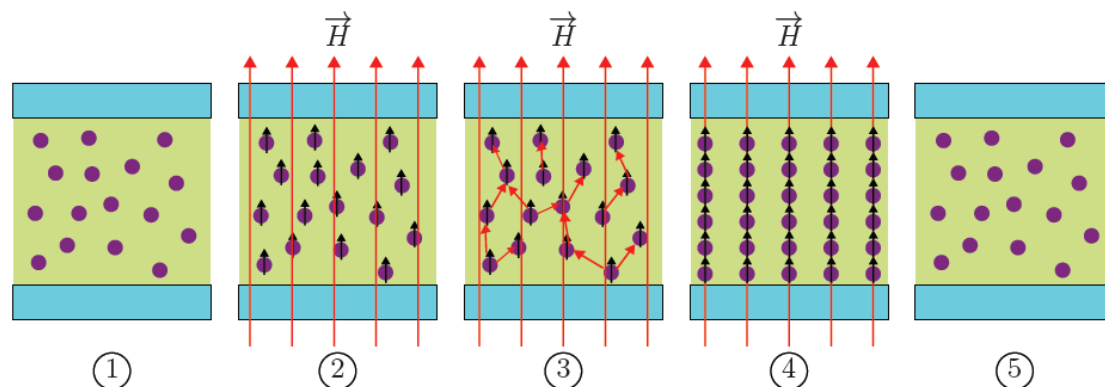
Figure 2-2: The particle chains formation stages and inducing the MR effect

This capability of MR fluids to develop a controllable yield stress which is proportional to the applied magnetic field provides a unique feature to interface mechanical systems with electrical devices in order to control vibration. The change in the yield stress due to the applied magnetic field is very fast and typically is in the order of milliseconds. Moreover the magnetic particles can aggregate even for a weak magnetic field (the order of 1 kA/m). The particles have a very small size so the magnetic dipole interaction energy between the particles of the MR fluid far exceeds the basics thermodynamic energy of thermal agitation.

The main use of MR fluids is to dissipate kinetic energy as heat. This process of energy dissipation can be controlled continuously and in real time using an electric signal. The electrical current applied to an electromagnet generates the activation magnetic field. Thus, the operation of the MR fluid systems is based on the generation of the magnetorheological effect within a certain portion of the air gap of constant section traversed by the liquid during an operating cycle.

The surfaces of the air gap through which the magnetic flux passes, also known as "poles" can be fixed or in relative movement with respect to each other. MR fluids may be operated in a variety of ways depending on the particular requirements of an application. The three common operational modes include valve mode, shear mode, and squeeze mode. For more information about these see Appendix A.

It should be noted that in comparison with their electro-rheological fluid counterparts, MR fluids can exhibit a higher order magnitude of yield stress (ranging between 50 and 100 kPa) and a wider operational temperature range (typically between -40°C to 150°C). Moreover, MR fluids are much less sensitive to the external contaminants.

The MR effect has been discovered by Rabinow in 1948 [Rabinow, 1948]. Despite the good performance of the first MR fluids in terms of mechanical strength [Carlson, 2002], they remained at the stage of experimental and theoretical studies. The reasons behind the inapplicability of MR fluids were difficulties in stabilizing the early formulations towards the sedimentation and irreversible agglomeration of particles [Phulé, 2001]. In the early 90s, advances in chemistry and condensed matter resulted in more stable formulations. Today, MR fluids are produced in large quantities and are used in a vast number of commercialized applications in the transportation industry and some more specific applications, such as protection against earthquakes, prosthetics and pneumatics.

2.1.2   Magnetorheological damper

2.1.2.1   Operating principle

MR damper design is inspired by those of conventional and hydraulic shock absorbers. But unlike hydraulic dampers, MR dampers do not require mechanical valves to control the flow. Instead, the two chambers are fully filled with a MR fluid and a magnetic field source (coil or magnet) is inserted into a portion of the system (piston) as shown in Figure 2-3. As the piston shaft enters the housing, MR fluid flows from the high pressure chamber to the low pressure chamber through the orifices in the piston head. The coil generates a magnetic field that interacts with the flowing fluid and causes the braking of the fluid flow. The MR effect modifies the rheological properties of the fluid as previously explained. This microscopic phenomenon continues to macroscopic scale by increasing the flow resistance, and thus the damping force.
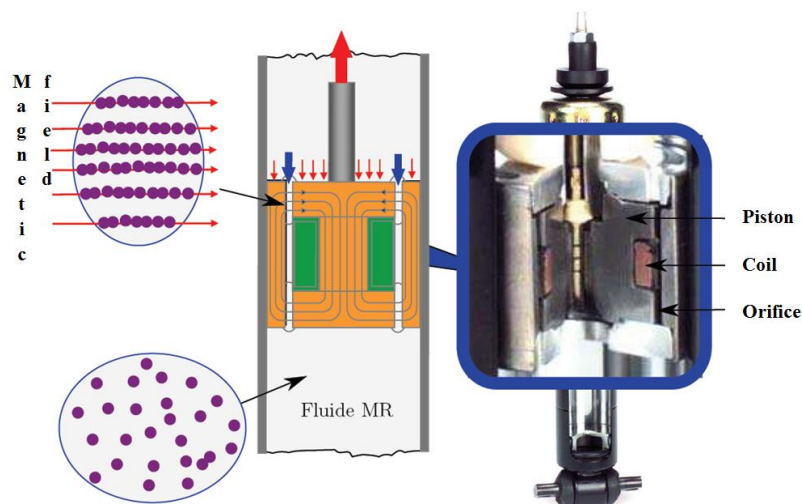
Figure 2-3: The principle of operation of an MR damper [Delphi, 2009].

2.1.2.2 Modeling of MR damper

The parametric damper models are formulated using rheological structures, which, in various ways, are used to approximate the MR fluid behaviour. Such models have direct influence on the accuracy of the damper behaviour prediction. Assuming, for example, the case that the MR fluid does not show any hysteresis, it may be treated as a visco-plastic material which leads to the Bingham model, or a visco-elastic material, which can lead to the Gamota-Filisko and Li models. However, in development of the MR fluids models, the appearance of hysteresis leads to the Bouc-Wen and Spencer models. In this section, the Bouc-Wen, proposed by [Wen, 1976], is presented since it is one of the most well-known models in this filed and implemented here. Appendix B provides more information about the Spencer model.

In the Bouc-Wen model, the hysteretic force is separated into two parts: linear and hysteretic sections. While, the later us expressed with the first order differential equation. The Bouc-Wen hysteresis model is well accepted in modelling of the MR dampers for its versatility. The schematic form of the Bouc-Wen model is shown in Figure 2-4.
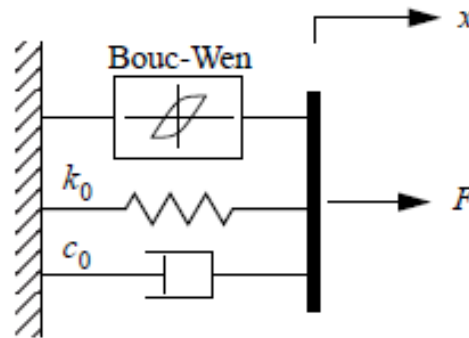
Figure 2-4: Rheological structure of a MR damper for the Bouc-Wen model [Spencer, 1996]

According to the proposed model, the damping force is given by equation (2-1)

$$F = c_0\dot{x} + k_0(x - x_0) + \alpha z \qquad (2\text{-}1)$$

Where k_0 and c_0 are damper stiffness and damping coefficients, respectively. α is the model funcional parameter and z is the evolutionary variable.

This variable should satisfy the equation (2-2) [Sapiński, 2003].

$$\dot{z} = -\gamma|\dot{x}|z|z|^{n-1} - \beta\dot{x}|z|^n + \delta\dot{x} \qquad (2\text{-}2)$$

Here n, δ, γ, β are parameters which determine the shape of the damping force hysteresis loop.

In general, the parameters n, A, γ are positive and β might be either positive or negative. The parameter n characterizes the smoothness of the force versus the displacement curve and in most of the applications $n = 1$ for different MR dampers. Usually, the parameters α, k, c are used to be polynomial functions of the applied current, I. The damping force-velocity curve in Figure 2-5 shows the influences of different parameters [Sapiński, 2003].
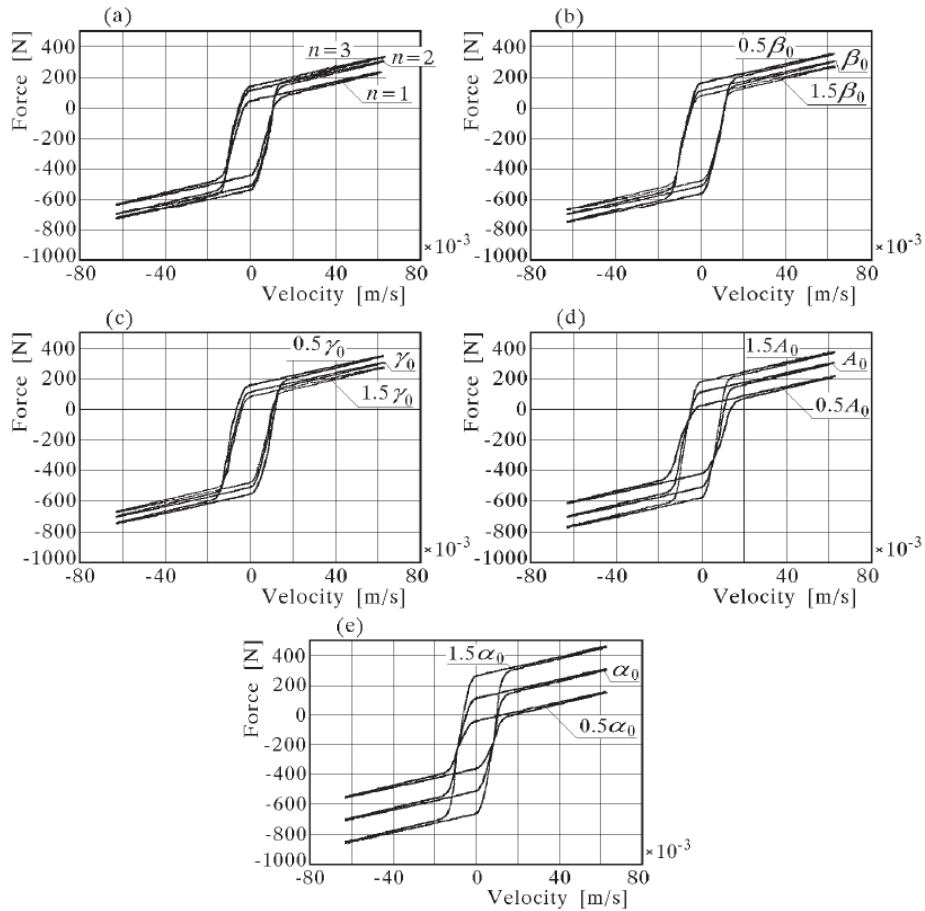
Figure 2-5: Influence of parameters n ,β, γ, A = δ and α on force-velocity curves [Sapiński, 2003]

A comparison between the predicted response and the corresponding experimental data is provided by [Sapiński, 2003] and shown in Figure 2-6. It proves that the Bouc-Wen model predicts the force-displacement behaviour of the damper with a satisfactory level of accuracy, and it possesses force-velocity behaviour that more closely resembles the experimental data. However, the nonlinear force-velocity response of the Bouc-Wen model does not roll-off in the region where the acceleration and velocity have opposite signs and the magnitude of the velocities are small.
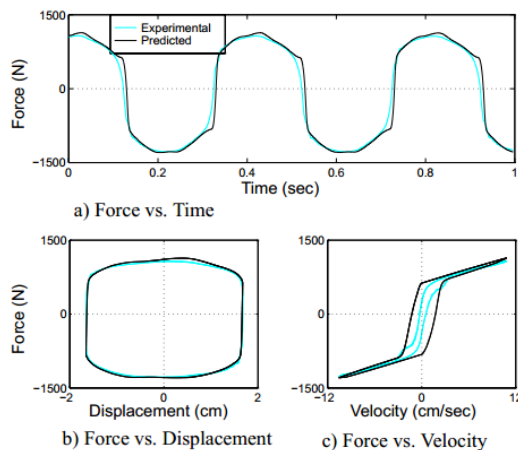
Figure 2-6: Comparison between the predicted and experimentally measured response for the Bouc-Wen model [Spencer, 1996]

2.2 Vibration control strategies

In this section, three main vibration control strategies called passive, semi-active and active are presented, briefly. More information regarding these control techniques can be found in [Ben Mekki, 2006], [Berbyuk, 2010], [Berbyuk, 2012] and [Sleiman, 2010].

2.2.1 Passive control

Passive techniques for structural vibration control use materials and components with intrinsic damping properties coupled to the structure so that the structural vibrations are damped passively (*i.e.*, without any additional external intervention or energy supply from outside of the system).

So a passive system is generally equipped using spring and dampers with constant stiffness and damping coefficients, respectively. The spring force depends on the elongation whereas the damper exerts a force according to the relative speed of the sprung mass $\dot{x}_2$ and the unsprung mass $\dot{x}_1$. In the case of the most common passive damper, the force generated by the damper (equation (2-3)) is assumed to be linearly dependent on the velocity.

$$F_{damper} = c(\dot{x}_2 - \dot{x}_1)$$
(2-3)

Where, c is the passive damping coefficient and assumed to remain constant.

Up to now, the passive damping technology is one the most well-known vibration control techniques and the standard hydraulic damper is the most widely used damper of this ilk. It already exists on the majority of the vehicles in automotive industry. Passive suspension suppresses the oscillations only by absorbing a part of the input energy. In passive suspension systems the damping characteristics vary only due to the wear of the elements during the operation. They have the same behaviour for all the input conditions. With this type of passive suspensions, some of the frequencies will not be filtered, properly and this is the most important drawback of such systems.

### 2.2.2 Active control

As explained before, a passive damper is designed primarily to reduce only a particular vibration mode of the system. In contrast, an active damper can absorb a wide band of frequencies. Hence, the study of active control systems is a logical extension of passive control technology. A control system is active if one or more actuators applying forces or torques to a structure according to a control law. Of course an external power supply is needed in this case to activate different components, such as sensors and actuators. Based on the operational condition, these actuating forces can be used to add or dissipate the energy to the structure in order to reduce vibrations. So these actuators can function either as controllable brake or motor, unlike the conventional damper used in the passive control which can only dissipate the energy.

The performance of an active control depends on how the actuator is controlled.

The example of the case studied in this work is taken to illustrate the active control (Figure 2-7).
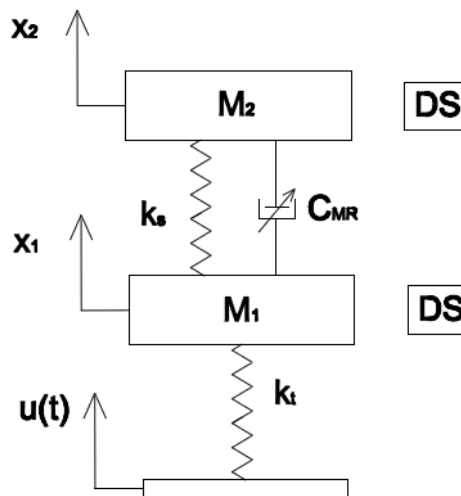
Figure 2-7: Illustrative example

A diagram of an active control system is shown in Figure 2-8.
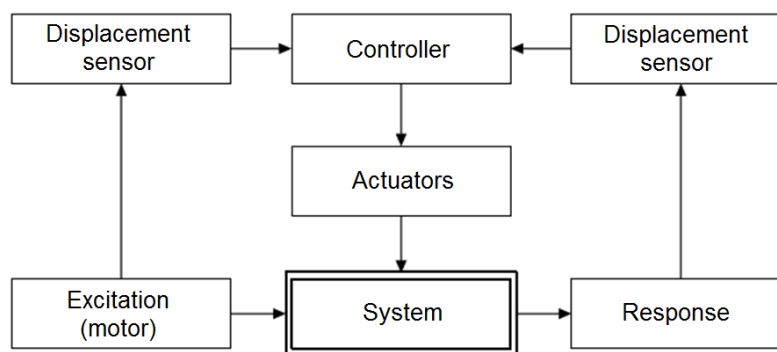
Figure 2-8: Diagram of an active control. As a first step, information as the velocity of the carts 1 and 2 are transmitted to the controller which calculates, according to a control strategy, the instruction necessary to the actuator. It acts on the system to reduce vibration. [Sleiman, 2010]

First, it involves displacement sensors (DS) on the cart 2 and on the cart 1, for measuring at each time step, the system response or the excitement coming from the engine. The second step is to choose a law and a suitable control strategy that allow the actuator to produce a force control.

The drawbacks of this method are mostly connected to high cost and complexity of the added mechatronic subsystem. Another critical issue with active control is the stability and robustness in the case of sensor failure.

2.2.3 Semi-active control

As its name suggests, the semi-active suspension is a compromise between passive and active systems. The main idea of semi-active control is very simple: it is to change, in real time, the characteristics of passive devices for energy dissipation and this change requires only minimal energy source. The concept of this type of control is introduced for the first time by [Karnopp, 1974] which proposes to amend the fluid damping force by controlling the opening of the valve of a conventional damper, for example, a hydraulic damper fitted a servo valve which controls the flow of oil through a restriction.

The control action for an approach to semi-active is realized through the adjustment in real time of mechanical parameters of dissipation reacts passively with the rest of the system. The modality of setting these parameters is determined on the basis of a choice of control algorithm, according to the excitation and / or the response of the system. Therefore, as for the active control, the semi-active control system requires sensors, processors and actuators. The energy required from the outside, by cons, is minimal compared to an active control system: only serves to modify the mechanical control devices, and can be provided, for example, by a simple battery. So semi-active control subsystems do not add mechanical energy to the system being controlled. Moreover they are usually less expensive to design and consume far less energy than devices for active vibration control. Therefore, systems of semi-active control represent an evolution of passive systems, they retain the fundamental characteristics of reliability, safety and ease, placing them next to the adaptation in order to increase its performances up to the active control systems.

2.3 Semi-active control algorithms

So the main focus is on the semi-active vibration control in this thesis. The damping coefficient of the MR damper varies between a minimum value and a maximum one. This coefficient is modified from a control algorithm, adjusting the mechanical properties of the control device to achieve significant reductions in system response amplitudes. The two most common control algorithms, Skyhook and Groundhook, are presented [Goncalves, 2001] to show the vibration suppression in the second and first cart, respectively. Finally, a third point is dedicated to define an alternative control based on the Skyhook and Groundhook.

2.3.1 Skyhook Control

The Skyhook configuration is shown in Figure 2-9. As the name implies, the mass m_2 is connected by a damper to a fixed point of reference in the sky. The Skyhook control focuses on the sprung mass when the base is excited by $u(t)$. Indeed, when the damping coefficient c_{sky} increases, the motion of m_2 decreases. This benefit involves a cost; the motion of the unsprung mass m_1 is then increased.
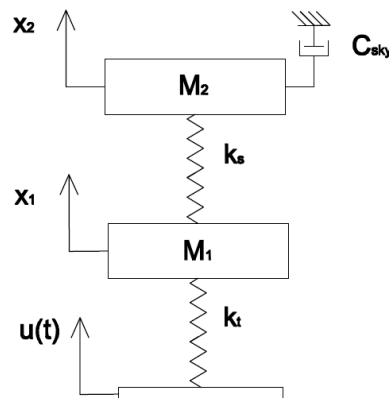
Figure 2-9: Skyhook ideal configuration

This configuration is not feasible when realistic automotive application has to be dealt. An alternative has been found by placing a semi-active damper between the sprung and the unsprung masses to achieve a similar result such as the one illustrated in Figure 2-10.
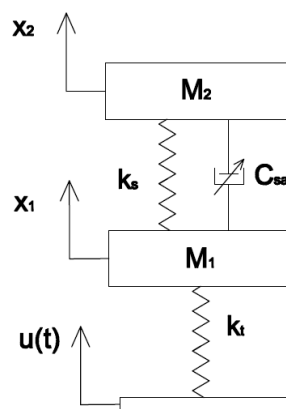
Figure 2-10: Semi-active equivalent model

With the experimental equipment available in this thesis, only the on-off Skyhook control strategy can be explored. This means that c_{sa} can only take two values: 0 (I_{off}) and c_{sky} (I_{on}). Now, the question is based on the current input condition in real time which coefficient should be applied and the MR damper should be on or off.

To answer this question, the most comprehensive way is to examine the forces on the sprung mass under different conditions. But first, certain parameters must be defined. Referring to Figure 2-10, the relative velocity $\dot{x}_{21}$ is defined as the velocity of the sprung mass m_2 relative to the unsprung mass m_1. When the two masses are separating $\dot{x}_{21}$ is positive. And for x_1, x_2, $u(t)$ and the forces, up is positive and down is negative.

The first case that is investigated here is when m_2 is moving upwards and the two masses are separating (Figure 2-11).

<div align="center">Ideal configuration   Semi-active equivalent model</div>
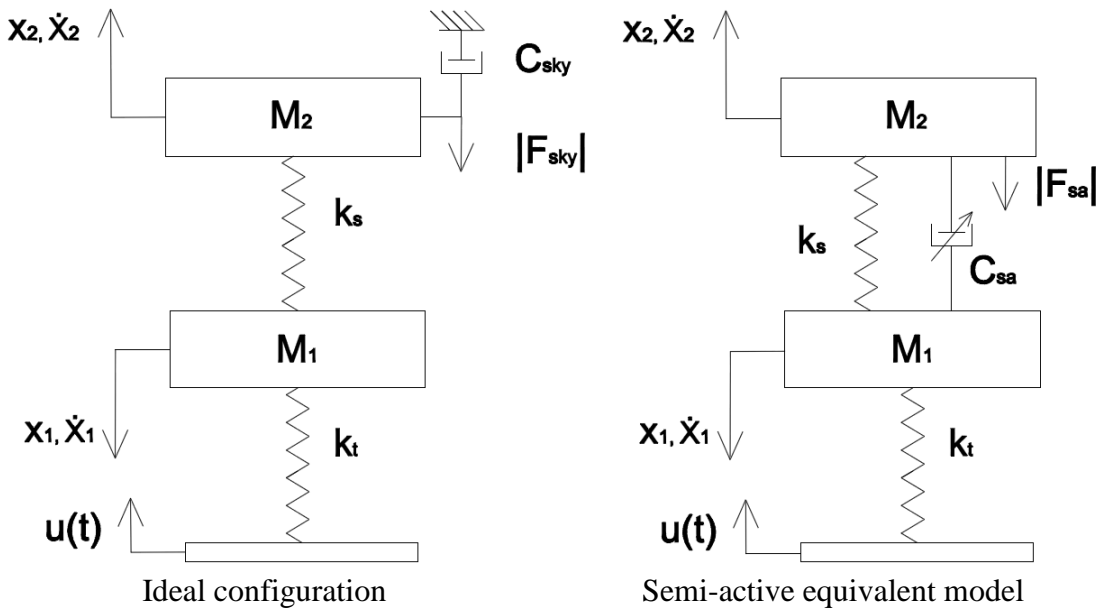
Figure 2-11: Illustration of the first case

Under the ideal Skyhook configuration, the force due to the Skyhook damper is equal to equation (2-4) [Goncalves, 2001].

$$F_{sky} = -c_{sky}.\dot{x}_2 \tag{2-4}$$

Where F_{sky} is the Skyhook damping force. Next, the semi-active equivalent model is examined and it appears that the damper is in tension and the damping force due to the semi-active damper is given by equation (2-5) [Goncalves, 2001].

$$F_{sa} = -c_{sa}.\dot{x}_{21} \tag{2-5}$$

Where F_{sa} is the semi-active damping force. Now, in order for the semi-active equivalent model to perform like the Skyhook model, equations (2-4) and (2-5) have to be equal:

$$F_{sky} = -c_{sky}.\dot{x}_2 = -c_{sa}.\dot{x}_{21} = F_{sa} \tag{2-6}$$

The semi-active damping can be isolated in the equation (2-6)

$$c_{sa} = \frac{c_{sky}.\dot{x}_2}{\dot{x}_{21}}$$
(2-7)

So the semi-active damping force is found (equation (2-8)) in the case when $\dot{x}_2$ and $\dot{x}_{21}$ are positive.

$$F_{sa} = c_{sky}.\dot{x}_2$$
(2-8)

The second case is when $\dot{x}_2$ and $\dot{x}_{21}$ are negative that means that m_2 is moving down and the two masses are coming closer (see, Figure 2-10). The skyhook damping force would be in the positive direction and is given by equation (2-9).

$$F_{sky} = c_{sky}.\dot{x}_2$$
(2-9)

Likewise, because the semi-active damper is in compression, the force due to the semi-active damper is also positive (equation (2-10)).

$$F_{sa} = c_{sa}.\dot{x}_{21}$$
(2-10)

The same procedure as for the first case is applied and the same semi-active damping is obtained. In conclusion, when the product of $\dot{x}_2$ and $\dot{x}_{21}$ is positive, the semi-active force is defined by equation (2-8).

The third case is when m_2 is moving upwards and the two masses are coming together. The force applied by the Skyhook damper on the sprung mass is again in the negative direction. But in this case, the semi-active damper compressed and so it cannot apply a force in the same direction as the Skyhook damper. Therefore, the damping has to be minimized to apply minimum force to the sprung mass.

Finally, the last case is when the sprung mass is moving downwards and the two masses are separating. The same situation as the previous case, therefore, the Skyhook damping force and the semi-active damping force are not in the same direction. So, the force on semi-active force should be minimized.

Resuming these four conditions, the Skyhook control policy can be written as equation (2-11) [Goncalves, 2001].

$$F_{sa} = \begin{cases} c_{sky}.\dot{x}_2 & if \quad \dot{x}_2.\dot{x}_{21} \geq 0 \\ 0 & if \quad \dot{x}_2.\dot{x}_{21} < 0 \end{cases}$$
(2-11)

It should be noted that the semi-active damper used in this study is a MR damper and the damping coefficient of this type of damper is directly proportional to the input current I going through the MR damper coil. Based on this fact, the equation (2-11) can be rewrite in terms of I_{on} and I_{off} (equation (2-12)).

$$I = \begin{cases} I_{on} & if \ \dot{x}_2.\dot{x}_{21} \geq 0 \\ I_{off} & if \ \dot{x}_2.\dot{x}_{21} < 0 \end{cases}$$
(2-12)

2.3.2 Groundhook control

The difference between the Groundhook and the Skyhook model is that instead of connecting the damper between the sprung mass and the sky, in the Groundhook configuration, the damper connects the unsprung mass and the ground (Figure 2-12). This structure is now focused on vibration suppression in the unsprung mass m_1. Indeed, the purpose is to isolate the unsprung mass from base excitations $u(t)$. The same as previous case with the Skyhook control, this performance comes at the cost of excessive vibration amplitudes in the sprung mass.
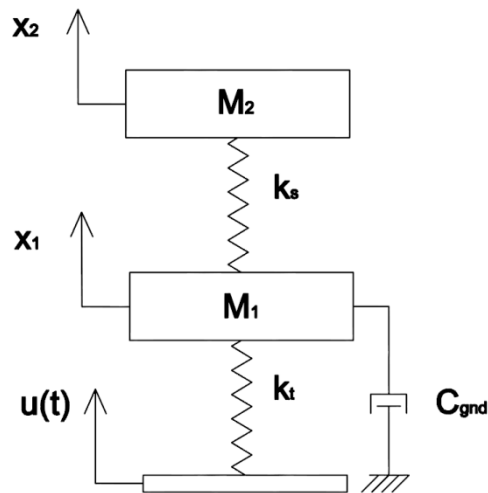
Figure 2-12: Groundhook ideal configuration

Like the previous case, this ideal configuration is not feasible for a realistic automotive application. So, the same alternative as the one considered for the Skyhook is used by placing a semi-active damper between the sprung and the unsprung masses as illustrated in Figure 2-10.

By reiterating the same reason for the Skyhook control described earlier, the Groundhook semi-active control can easily be found as the policy of equation (2-13) [Goncalves, 2001].

$$I = \begin{cases} I_{on} & if\ \dot{x}_1.\dot{x}_{12} \geq 0 \\ I_{off} & if\ \dot{x}_1.\dot{x}_{12} < 0 \end{cases} \tag{2-13}$$

2.3.3 Alternative Skyhook and Groundhook control algorithms

Based on the Skyhook and Groundhook concepts, several semi-active control strategies have been discovered during the last decades. The ultimate goal of this work is also to explore the advantages and disadvantages of each case both theoretically and experimentally and finally clarify those semi-active control techniques that show the best performance in comparison with the corresponding passive case. The physical representation of these controls remains unchanged from the conventional semi-active configuration shown in Figure 2-10.

Goncalves [Goncalves, 2001] proposed two alternatives to the Skyhook control. In order to improve the skyhook method the governing condition by which the damper input current is applied has been modified. The first alternative is a displacement and relative velocity based algorithm and can be expressed by equation (2-14)

$$I = \begin{cases} I_{on} & if \ x_2.\dot{x}_{21} \geq 0 \\ I_{off} & if \ x_2.\dot{x}_{21} < 0 \end{cases} \tag{2-14}$$

The second alternative suggested by [Goncalves, 2001] is the velocity and relative displacement based Skyhook algorithm and is described as equation (2-15).

$$I = \begin{cases} I_{on} & if \ \dot{x}_2.x_{21} \geq 0 \\ I_{off} & if \ \dot{x}_2.x_{21} < 0 \end{cases} \tag{2-15}$$

Then [Koo, 2003] proposed an alternative to the Groundhook control. It is based on the same condition of the first alternative to the Skyhook exposed previously. I.e., it is a displacement and relative velocity based Groundhook algorithm and can be expressed by equation (2-16)

$$I = \begin{cases} I_{on} & if \ x_1.\dot{x}_{12} \geq 0 \\ I_{off} & if \ x_1.\dot{x}_{12} < 0 \end{cases} \tag{2-16}$$

In this study, a new case is treated. It is the velocity and relative displacement based Groundhook algorithm and is described as equation (2-17). This strategy is obtained by applying the same modification done on the Skyhook algorithm given by equation (2-15). It means that, instead of using the relative velocity of the regular Groundhook (equation (2-13)), the relative displacement is employed.

$$I = \begin{cases} I_{on} & if \ \dot{x}_1.x_{12} \geq 0 \\ I_{off} & if \ \dot{x}_1.x_{12} < 0 \end{cases} \tag{2-17}$$

Finally, the last control that will be implemented is the one suggested by [Rakheja, 1985]. Which works based on the relative velocity and relative displacement strategy given by equation (2-18).

$$I = \begin{cases} I_{on} & if \ \dot{x}_{21}.x_{21} \geq 0 \\ I_{off} & if \ \dot{x}_{21}.x_{21} < 0 \end{cases} \tag{2-18}$$

3   Case study

In this section, the experimental test rig used in this study is introduced and different components are discussed, briefly.

3.1 Multi-cart system

The multi-cart system test rig that is utilized in this thesis is shown in Figure 3-1. This experimental set-up is designed and manufactured by the mechanical systems research group and is available at the vibration and smart structure laboratory, Chalmers University of Technology.
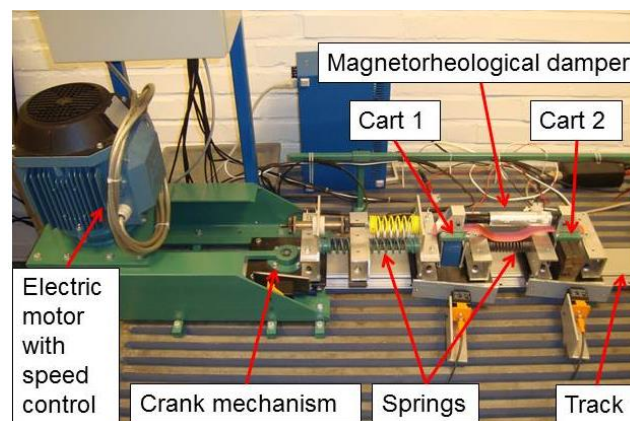
Figure 3-1: Multi-cart system test rig

The test rig is composed of the following elements:

- ➢ Two carts, car 1 and 2, that can slide on a track.

- ➢ Helical springs that connect the electric motor and carts.

- ➢ An electric motor with speed control which excites the system and sets the carts in motion through a crank mechanism. Notice that the motor used in this test rig came from ABB Group. Its model is M3AA 112M 6. It is a three phases motor with six poles using an alternative current of 440 V and it provides a power of 2.2 kW

- ➢ Different semi-active control strategies are explored using a magneto-rheological damper that connects the carts.

Notice that this system could be equivalent to a quarter-car system that is placed horizontally. In other words, road irregularities are estimated by the excitations coming from the electric motor, the first and second carts are considered as the vehicle's wheel and chassis, respectively. Therefore, application of MR damper in vibration control of an automotive vehicle can be estimated by this test-rig.

3.2 Magnetorheological damper

The MR damper that is used in this test rig is the RD-1097-01 damper from Lord Corporation (Figure 3-2).
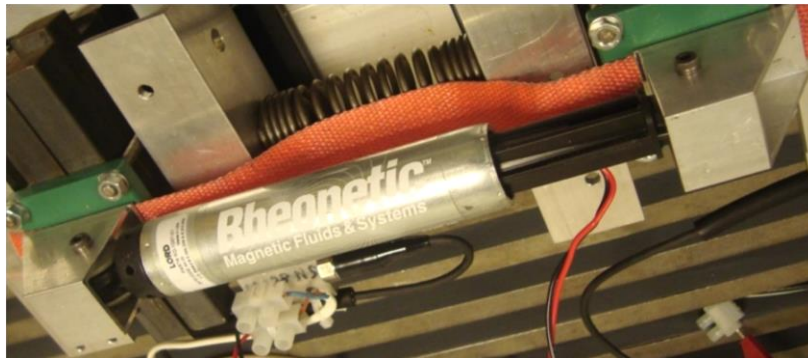
Figure 3-2: Lord Corporation MR damper

This MR damper is a sponge-type MR fluid damper. Three other types of MR dampers exist on the market and are described in Appendix C.

The sponge-type damper (presented by [Zhu, 2012]), in which the MR fluid is contained in an absorbent matrix, employs the shear mode operation with less complexity and seal problems. As shown in Figure 3-3, the outer cylinder is a hollow steel tube and the piston head is comprised of an open-celled polyurethane foam saturated with MRFs and an electromagnet that generates the yielding shear force resisting the motion of the piston within the cylinder. Sponge-type MRF dampers could be operated in a direct shear mode without seals, bearings, or precise mechanical tolerances and only requiring a minimum volume of MRFs, which facilitates the application of MRFs in cost-sensitive areas. In practice, a low-cost, sponge-based MRF damper has been utilized in high-performance washing machines [Hoyle, 2010]. The feasibility of sponge-based force feedback MRF dampers for telerobotic systems was investigated in a study recently [Ahmadkhanlou, 2008].
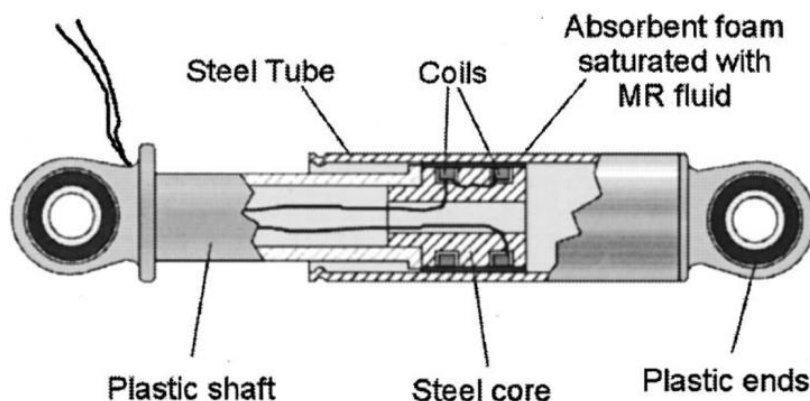
Figure 3-3: Schematic configuration of a sponge-type MR fluid damper [Yoshioka, 2002]

Technical characteristics of the MR damper used in this research are given by Table 3-1 [Nyman, 2008]:

Table 3-1: Characteristics of the MR damper

Property	Value
Extended length	253 mm
Compressed length	195 mm
Diameter	32 mm
Weight	0,48 kg
Stroke	50 mm
Input voltage	12V DC
Continuous input current	$< 0,5$ A
Intermittent input current	$< 1,0$ A
Coil resistance	20 Ω
Damper force (peak to peak)	100 N (50 mm/s, 1 A) 2 N (200 mm/s, 0 A)
Operating temperature	$< 70°C$
Reaction time*	< 25 ms
Life-span**	2 million cycles

*   Time to reach 90% of the maximum level (varies with amplifier and power supply)

**   At 26 mm stroke, 2 Hz, current varying between 0 and 0.5 A

4 Mathematical model

In this section, the equations of motions for the two-cart experimental set-up described in the previous chapter are derived. Application of different semi-active vibration control strategies using MR damper discussed in the previous chapters is shown, mathematically. The results are compared with the corresponding passive case to exhibit the improvement in vibration suppression for each particular strategy.

4.1 Theory

Figure 4-1 shows the two degrees of freedom (DOFs) model, which is comprised of a sprung mass m_2, an unsprung mass m_1, three springs having stiffness of k_1, k_2 and k_3, respectively. The MR damper effects are substituted by a force **F** that is applied on both carts, the viscous dampers are there to take into account the energy dissipation by friction between the carts and the track and they have a damping coefficient of c. $\mathbf{u(t)}, x_1$ and x_2 are the displacement of the motor excitation, unsprung mass and sprung mass, respectively.
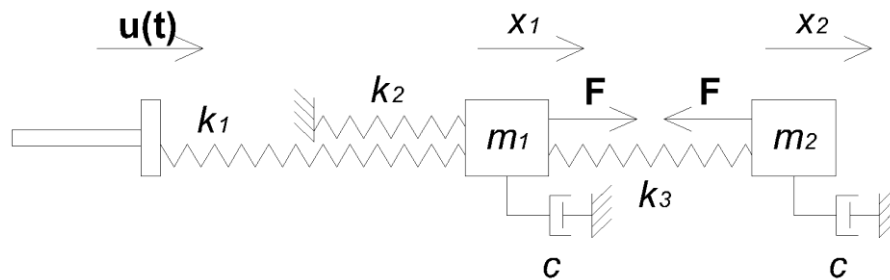
Figure 4-1: Mechanical model of the test rig

The dynamic equations of motion for this 2-DOF model are given by equation (4-1):

$$\begin{bmatrix} m_1 & 0 \\ 0 & m_2 \end{bmatrix} \cdot \begin{Bmatrix} \ddot{x}_1 \\ \ddot{x}_2 \end{Bmatrix} + \begin{bmatrix} c & 0 \\ 0 & c \end{bmatrix} \cdot \begin{Bmatrix} \dot{x}_1 \\ \dot{x}_2 \end{Bmatrix} + \begin{bmatrix} k_1+k_2 + k_3 & -k_3 \\ -k_3 & k_3 \end{bmatrix} \cdot \begin{Bmatrix} x_1 \\ x_2 \end{Bmatrix} = \begin{bmatrix} \mathbf{F} + k_1 \cdot \mathbf{u(t)} \\ -\mathbf{F} \end{bmatrix} \qquad (4\text{-}1)$$

In equation (4-1), F is given by the Bouc-Wen model presented before.

The first step is to determine the properties of the test rig. This is necessary for comparison of the experimental and mathematical results.

The carts were weighted and here is the mass matrix:

$$\mathbf{M} = \begin{bmatrix} 3.485 & 0 \\ 0 & 6.745 \end{bmatrix} kg \qquad (4\text{-}2)$$

In order to define the stiffness matrix, the stiffness coefficient is determined using the following formula:

$$k = \frac{F}{(l - l_0)} \qquad (4\text{-}3)$$

Where, l is the elongation of the spring and l_0 is the initial elongation of the spring.

To attain all the necessary measurements associated with the mass and spring properties, the following system shown in Figure 4-2 is used. The Table 4-1 summarizes the calculated stiffness of all springs:

Table 4-1: Stiffnesses of the springs used in the test-rig

Stiffness	Value (N/m)
k_1	7600
k_2	4800
k_3	7500

Figure 4-2: Estimation of stiffness values

From Equation (4-1), the resulting stiffness matrix is as follows:

$$\mathbf{K} = \begin{bmatrix} 19900 & -7500 \\ -7500 & 7500 \end{bmatrix} N/m \tag{4-4}$$

Once the mass and stiffness matrix are known, the Eigenfrequencies can be calculated using the MATLAB code below:

```
lambda = eig(inv(K)*M)
poles = 1./sqrt(lambda)
f = poles/(2*pi)
```

So the first Eigenfrequency (system resonance or natural frequency) is 4 Hz and the second one is 12.5 Hz. To confirm that the results are correct, the motor speed (in the test-rig shown in Figure (3-1)) to excite the system on a frequency range that cover the systems' natural frequencies. The speed increased till the two resonance frequencies appeared. The first one showed up at 4 Hz and the second one around 12 Hz. It proves that the theoretical results are consistent with the experiment.

As a result of some sort of difficulties, the damping coefficient c could not be calculated directly from the experimental data. therefore, an estimation has been made on the damping matrix and it is written below:

$$\mathbf{C} = \begin{bmatrix} 4.65 & 0 \\ 0 & 4.65 \end{bmatrix} Ns/m \tag{4-5}$$

4.2 MATLAB code

Once the system properties are known, the mathematical model is implemented in MATLAB to compare the different control algorithms.

The system of equations given by equation (4-1) can be solved using the ODE45 function in MATLAB. But, first the two second order differential equations have to be rewritten in terms of four first order differential equations to be able to solve using ODE45. In fact, the system equations of motion should be written in the state space form.

The first step is to define the new coordinates such as:

$$z_1(t) = x_1(t) \quad z_3(t) = \dot{x}_1(t) \quad \dot{z}_1(t) = z_3(t)$$
$$z_2(t) = x_2(t) \quad z_4(t) = \dot{x}_2(t) \quad \dot{z}_2(t) = z_4(t) \tag{4-6}$$

the initial conditions should also be modified as given by equation (4-7):

$$z_1(0) = 0 \quad \dot{z}_1(0) = 0$$
$$z_2(0) = 0 \quad \dot{z}_2(0) = 0 \tag{4-7}$$

under such conditions, the system given by equation (4-1) is rewritten as:

$$\begin{cases} \dot{z}_3 = \dfrac{1}{m_1}[-(k_1 + k_2 + k_3).z_1 + k_3.z_2 - c.z_3 + F + k_1.u] \\[2mm] \dot{z}_4 = \dfrac{1}{m_2}[k_3.z_1 - k_3.z_2 - c.z_4 - F] \end{cases} \tag{4-8}$$

This system is written in the following compact state space form:

$$\dot{\mathbf{z}} = \mathbf{A}.\mathbf{z} + \mathbf{B}.\mathbf{u} + \mathbf{B_{MR}}.\mathbf{F} \tag{4-9}$$

Where:

> $$\mathbf{A} = \begin{bmatrix} 0 & I \\ \mathbf{M}^{-1}.\mathbf{K} & -\mathbf{M}^{-1}.\mathbf{C} \end{bmatrix}, \quad \mathbf{B} = \begin{bmatrix} 0 \\ 0 \\ \dfrac{k_1}{m_1} \\ 0 \end{bmatrix}, \quad \mathbf{B_{MR}} = \begin{bmatrix} 0 \\ 0 \\ \dfrac{1}{m_1} \\ -\dfrac{1}{m_2} \end{bmatrix} \tag{4-10}$$

> **u** is the excitation.

In the mathematical model, two types of excitations are implemented to see if the control strategies have the same influence on the vibration isolation. The first one is the harmonic excitation produced by the motor to excite the system within a range of frequencies. The kinematic input introduced by the motor in this case is given as a frequency-ramp function given by equation (4-11).

$$\mathbf{u(t)} = a.\sin(2.\pi.f.t) \ where \ \begin{cases} a = 0.0065 \, m \\ f = frequency \\ t = time \end{cases} \tag{4-11}$$

Figure 4-3 shows the evolution of the motor frequency during one ramp. This means that the frequency increases from 0 to 10 Hz between 0 and 10 seconds, then decreases to 0 Hz between 10 and 20 seconds. The choice of this value will be explained in the next sections dedicated to the LabView code.
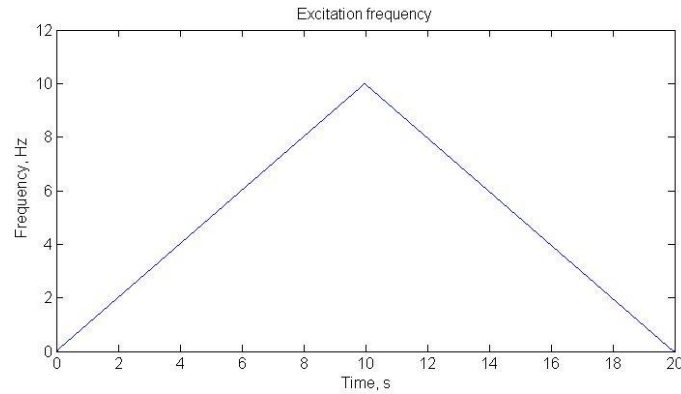
Figure 4-3: Evolution of the excitation frequency

The second excitation is modelled as an impact force. That means for a short time period the excitation reaches a maximum value. This can be modelled by a step function on a short time given by equation (4-12).

$$\mathbf{u(t)} = \begin{cases} a & if \quad 1 \leq t \leq 1.05 \\ 0 & else \end{cases} \qquad (4\text{-}12)$$

This excitation is illustrated by Figure 4-4.
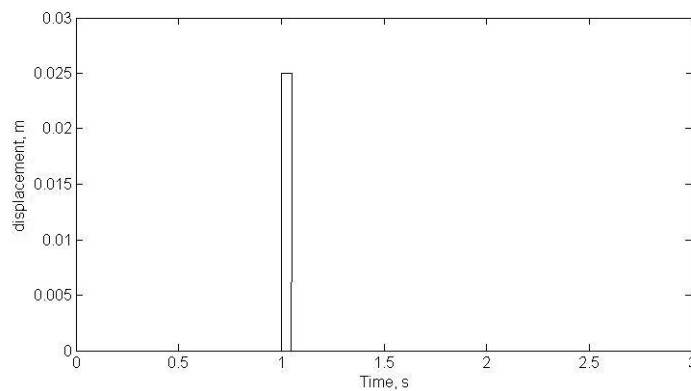
Figure 4-4: Modelling of the hammer blow

➢ **F** is the force applied by the MR damper.

As explained before the model chosen to represent it is the Bouc-Wen model.

For a particular MR damper, the damping force is given by equation (4-12)

$$\mathbf{F} = c(I).\dot{x} + k.x + \alpha(I).\mathbf{q} \qquad (4\text{-}13)$$

Where x is the elongation of the damper, $k = 0 \, N/m$, and the variables $c(I), \alpha(I)$ depend on the applied current and are given by the following expressions [Berbyuk, 2010]:

$$c(I) = 0.002 + 0.0017\,I^3 \tag{4-14}$$

$$\alpha(I) = 2.2310 + 53.971\,I + 22.8329\,I^2 + 0.0067\,I^3 \tag{4-15}$$

Finally the evolutionary variable $\mathbf{q}$ is introduced as an additional state which satisfies the equation (4-16)

$$\dot{\mathbf{q}} = \delta\dot{x} - \gamma|\dot{x}|\mathbf{q} - \beta\dot{x}|\mathbf{q}|, \qquad \mathbf{q(0)} = 0 \tag{4-16}$$

The particular MR damper used in this thesis has been studied during a bachelor thesis [Nyman, 2008] in order to determine different parameters of the equation (4-16). Table 4-2 sums up the results:

Table 4-2: Bouc-Wen parameters as a function of the input current

Current (A)	β	γ	δ
0.00	-3.5298	7.8538	15.6516
0.15	-3.5702	7.5116	16.7951
0.30	-3.7093	6.8963	16.6925
0.45	-3.5525	6.7611	16.7966
0.65	-3.5432	6.7118	17.4905

The ODE45 is also used for solving the first order differential equation introduced by the Bouc-Wen model.

The last step is to implement several semi-active control algorithms shown in Table 4-3.

Table 4-3: On-off semi-active control algorithms

	Skyhook	Groundhook
Velocity and relative velocity based	$I = \begin{cases} I_{on} & if\ \dot{x}_2.\dot{x}_{21} \geq 0 \\ I_{off} & if\ \dot{x}_2.\dot{x}_{21} < 0 \end{cases}$	$I = \begin{cases} I_{on} & if\ \dot{x}_1.\dot{x}_{12} \geq 0 \\ I_{off} & if\ \dot{x}_1.\dot{x}_{12} < 0 \end{cases}$
Displacement and relative velocity based	$I = \begin{cases} I_{on} & if\ x_2.\dot{x}_{21} \geq 0 \\ I_{off} & if\ x_2.\dot{x}_{21} < 0 \end{cases}$	$I = \begin{cases} I_{on} & if\ x_1.\dot{x}_{12} \geq 0 \\ I_{off} & if\ x_1.\dot{x}_{12} < 0 \end{cases}$
Velocity and relative displacement based	$I = \begin{cases} I_{on} & if\ \dot{x}_2.x_{21} \geq 0 \\ I_{off} & if\ \dot{x}_2.x_{21} < 0 \end{cases}$	$I = \begin{cases} I_{on} & if\ \dot{x}_1.x_{12} \geq 0 \\ I_{off} & if\ \dot{x}_1.x_{12} < 0 \end{cases}$
Relative velocity and relative displacement based	$I = \begin{cases} I_{on} & if\ \dot{x}_{21}.x_{21} \geq 0 \\ I_{off} & if\ \dot{x}_{21}.x_{21} < 0 \end{cases}$	

Where in this table, I is the current applied to the MR damper, x_1 and x_2 are displacements, and $\dot{x}_1$ and $\dot{x}_2$ are velocities of cart 1 and cart 2, respectively. x_{21} is equal to $x_2 - x_1$ and x_{12} is equal to $x_1 - x_2$ and the same relations can be applied to the velocities. It should be noted that the relative velocity and relative displacement based strategies are the same for the Skyhook and the Groundhook.

Within the frame of existing test-rig, only zero and maximum allowed damper input electrical current can be applied to the MR damper as I_{off} and I_{on}, respectively. So the main focus in MATLAB code is on the implementation of on-off strategies. However, a continuous Skyhook algorithm base on velocity and relative velocity is also added to the code in order to exhibit the advantages compared to the on-off approach. Equation (4-17) presents the continuous Skyhook algorithm:

$$I = \begin{cases} I_{cont} & if\ \dot{x}_2 . \dot{x}_{21} \geq 0 \\ I_{off} & if\ \dot{x}_2 . \dot{x}_{21} < 0 \end{cases} \tag{4-17}$$

In equation (4-17), I_{cont} belongs to $[I_{off}, I_{on}]$ and is found by solving the equation (4-18).

$$\min_{I_{cont} \in [I_{off}, I_{on}]} (F(I_{cont}) - F_{sky}) \tag{4-18}$$

Equation (4-18) means that I_{cont} should minimize the difference between $F(I_{cont})$, the force developed by the MR damper when I_{cont} is applied, and F_{sky}, the ideal force that has to be applied and is equal to $c_{sky} . \dot{x}_2$. Where, c_{sky} is a control model parameter and for the case studied is equal to 100 Ns/m. In other words, I_{cont} is optimized to minimize the deviation of the force developed by the MR damper ($F(I_{cont})$) and the corresponding ideal force (F_{sky}).

4.3 Results

The solution to equation (4-9) is the dynamics response of the system. In order to compare the efficiency of each control strategy, the RMS values of the carts at the displacement, velocity and acceleration levels are computed. Of course, smaller values of that parameter denote smaller amplitude of oscillations and higher control efficiency. First, the results associated with the first excitation type are examined. The reference case is the passive control using the optimized value of the input electrical current. Therefore, the first task is to determine the current for which the RMS values of displacement, velocity and acceleration are the lowest. Simulations are run with I varying from 0 to 0.5 A with increments of 0.01A because of the standard working range of the MR damper. The results are collected in Table 4-4.

Table 4-4: RMS values of the system response for the optimized values of the input current

	I (A)	x (m)	I (A)	$\dot{x}$ (m/s)	I (A)	$\ddot{x}$ (m/s²)
Cart 1	0.50	0.0109	0.50	0.8050	0.50	64.4385
Cart 2	0.22	0.0094	0.21	0.3006	0.49	16.1915

For most of the cases, Table 4-4 shows that the optimum current is around 0.50 A (*i.e.* max MR damper design current value). In order to compare the theoretical results with the corresponding experimental results, I_{on} is chosen equal to 0.47 A (For more information about this refer to Section 5.3). In the subsequent sections of this report, these optimized RMS values obtained by the passive control are compared with the semi-active strategies results using $I_{on} = 0.47\ A$.

Figure 4-5 shows displacements, velocities and accelerations of cart 1 and cart 2 for the passive case using $I_{on} = 0.47\ A$.
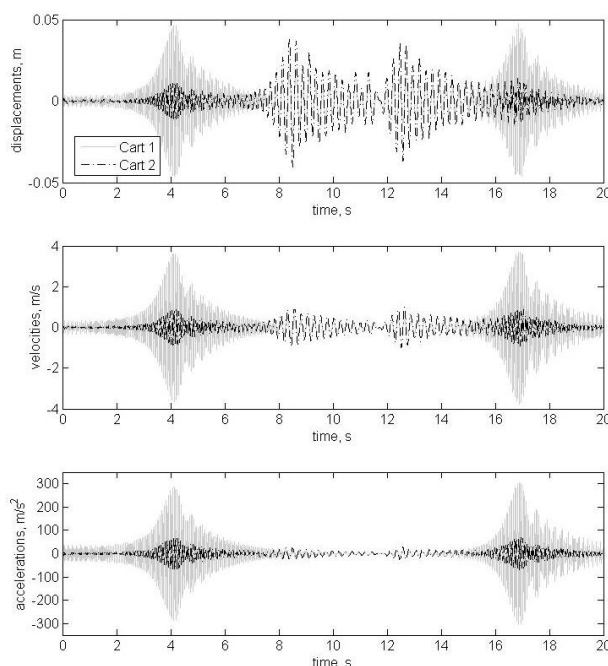

Figure 4-5: Displacements, velocities and accelerations of cart 1 and cart 2 using passive control under the first excitation type.

Since it is not feasible to compare the time domain results in different cases, the RMS values of positions, velocities and accelerations are compared. The Table 4-5 sums up these values for all algorithms that are implemented.

Table 4-5: RMS values for different algorithms

	Position (m)		Velocity (m/s)		Acceleration (m/s^2)	
Strategy	Cart 1	Cart2	Cart 1	Cart2	Cart 1	Cart2
Passive	0.0109	0.0098	0.810	0.310	64.8	16.2
V2V21	0.0110	0.0095	0.819	0.304	65.4	16.2
Cont Sky	0.0101	0.0085	0.750	0.271	59.6	14.4
P2V21	0.0093	0.0086	0.686	0.264	54.6	13.4
V2P21	0.0092	0.0083	0.678	0.257	54.0	13.2
V21P21	0.0092	0.0085	0.675	0.262	53.7	13.3
V1V12	0.0109	0.0096	0.812	0.302	65.0	16.1
P1V12	0.0095	0.0096	0.687	0.287	54.5	13.7
V1P12	0.0095	0.0103	0.678	0.299	53.8	13.7

In order to have a better representation of the results, the relative improvement (Γ_{rel}) associated with each semi-active strategy with respect to the corresponding passive case is illustrated by calculating the relative variation of the RMS values of the semi-active strategy results and the RMS values of the passive control defined by the equation (4-19):

$$\Gamma_{rel}(\%) = \frac{RMS_{semi-active} - RMS_{passive}}{RMS_{passive}} \times 100 \qquad (4\text{-}19)$$

Results of such comparison are given in Figure 4-6 for different cases. The x-axis denotes several control techniques implemented in this study while the y-axis shows the improvement w.r.t the passive control in percentage. Part (a) shows the results for the cart 1 and part (b) one exhibit the results for the cart 2.
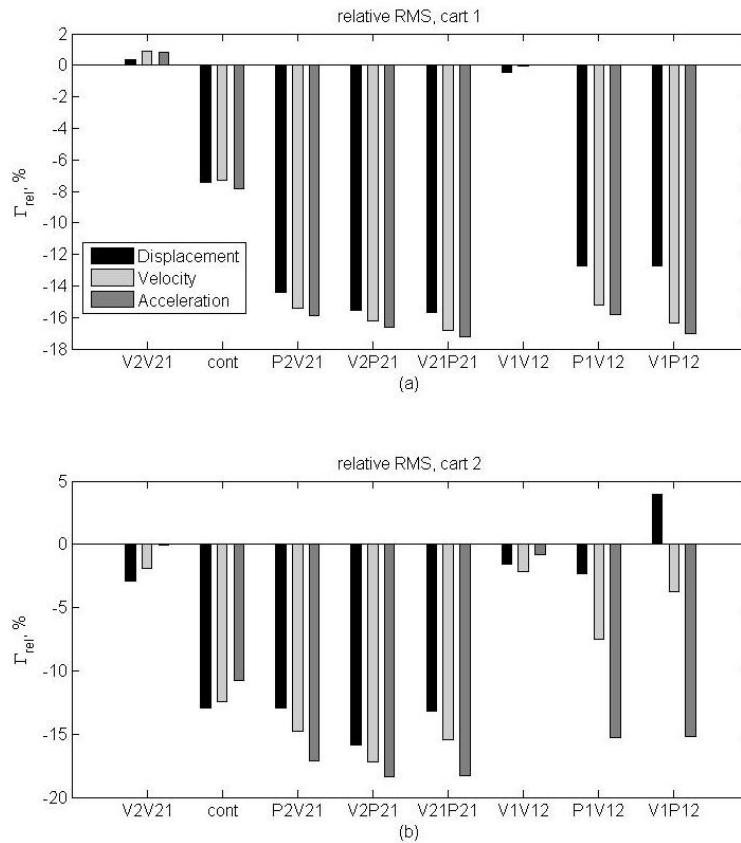
Figure 4-6: Improvement of the semi-active control results compare to the passive case in ramp excitation

What follows can be concluded from Figure 4-6: First, the on-off Skyhook approach based on the velocity and relative velocity (V2V21) is examined. As expected this strategy caused the vibrations of cart 1 to increase, slightly and vibrations of cart 2 to reduce. However, from Figure (4-6) it is obvious that the improvement is not significant.

Second, the other Skyhook strategies, P2V21 and V2P21, that again are employed to decrease the vibrations of cart 2, act much more efficiently than the V2V21 strategy. Indeed, the improvement is five times the one provided by V2V21. Furthermore, these strategies are not only effective on vibration suppression of cart 2 but also on cart 1.

Third, the Groundhook approach based on the velocity and relative velocity, V1V12, does not show the expected results. In fact, according to the theory, vibrations of cart 1 should decrease while for the case of cart 2 should increase slightly. However, the results given in Figure (4-6) have shown a decrease in the motion of both carts. This is due to the fact that the second Eigenfrequency of the system is not reached during the excitation. Generally, semi-active algorithms show the expected action in terms of vibration isolation at the resonances of the system. The modified Groundhook algorithms (P1V12 and V1P12), on the other hand, not only provide very good results on vibration suppression of cart 1, but also in acceleration of cart 2 w.r.t the passive case.

Fourth, the control strategy based on the relative velocity and relative displacement (V21P21) has shown brilliant results in vibration reduction of both carts.

Finally, when the velocity and relative velocity algorithm (V2V21), is used with the continuous Skyhook scheme, the improvement is four to five times compared to the

passive scheme. So it would be interesting to implement the same strategies, but using the continuous scheme instead of the on-off approach to see if more improvement is achieved.

The power spectral densities for the model are displayed in Figure 4-7. Graphs (a) and (b) are related to cart 1 and graphs (c) and (d) to cart 2. Graphs (a) and (c) are shown the first Eigenfrequency zone, i.e. 4.15 Hz while graphs (b) and (d) exhibit the second resonance frequency, *i.e.* 12.7 Hz.

(a)   (b)

(c)   (d)
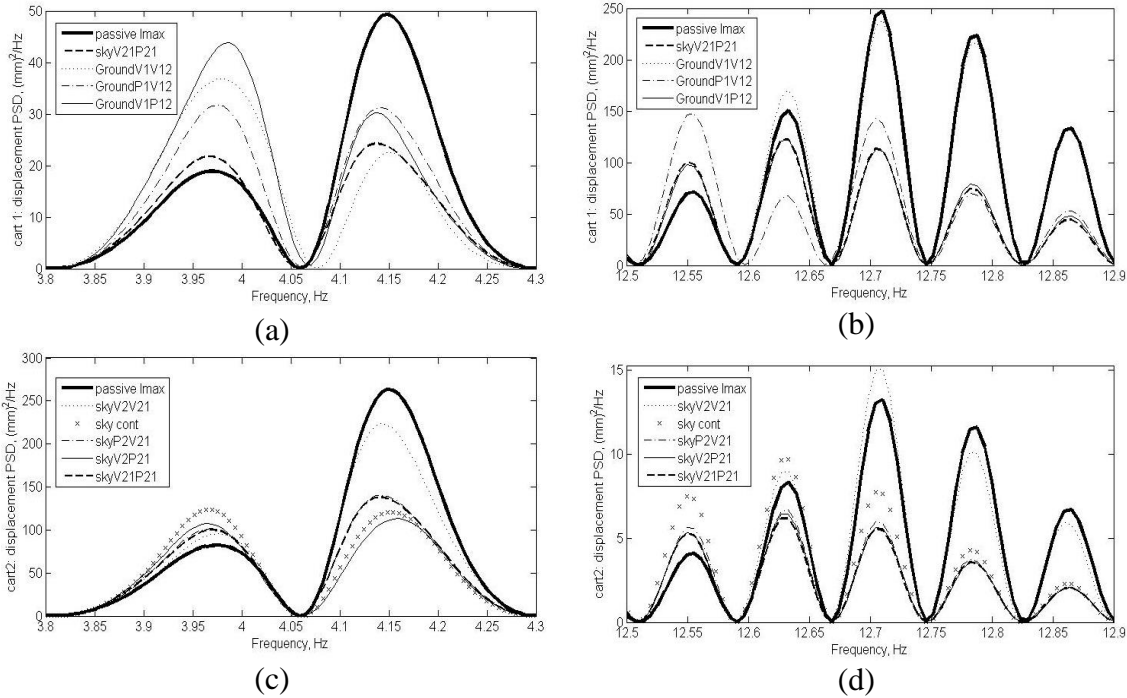
Figure 4-7: Power spectral density for the carts' displacements in ramp excitation.

From the vibration isolation point of view, Figure 4-7 shows that the semi-active control strategies are much more effective than the passive one around the resonance frequency.

As a conclusion, Table 4-6 recapitulates the two best vibration control strategies for each given case.

Table 4-6: Vibration control algorithms with highest efficiency

Position (m)		Velocity (m/s)		Acceleration (m/s²)	
Cart 1	Cart2	Cart 1	Cart2	Cart 1	Cart2
V2P21	V2P21	V21P21	V2P21	V21P21	V2P21
V21P21	V21P21	V1P12	V21P21	V1P12	V21P21

Let's now compare these best semi-active strategies with the optimized passive control to see if there is still improvement. Table 4-7 sums up the best strategies for vibration reduction in cart 1 (given in Table 4-6) and Table 4-8 is shown the corresponding results for cart 2.

Table 4-7: Vibration control improvements of cart 1 for the best semi-active strategies w.r.t the optimized passive control

Position (m)		Velocity (m/s)		Acceleration (m/s²)	
Strategy	Improvement	Strategy	Improvement	Strategy	Improvement
V2P21	-15.3 %	V21P21	-16.1 %	V21P21	-16.7 %
V21P21	-15.3 %	V1P12	-15.8 %	V1P12	-16.5 %

Table 4-8: Vibration control improvements of cart 2 for the best semi-active strategies w.r.t the optimized passive control

Position (m)		Velocity (m/s)		Acceleration (m/s²)	
Strategy	Improvement	Strategy	Improvement	Strategy	Improvement
V2P21	-11.7 %	V2P21	-14.5 %	V2P21	-18.5 %
V21P21	-8.9 %	V21P21	-12.8 %	V21P21	-17.8 %

In these cases, Tables (4-7) and (4-8) show that the semi-active control strategy can improve the performance up to 18% in comparison with the optimized passive control. In addition, such semi-active approaches consume less energy since the damper should not be always on (like the passive case using MR dampers). Such features make the semi-active vibration control using MR dampers one of the most efficient vibration control techniques that could be used in a variety of industries, such as automotive, rail and so on.

Now, let's analyse the results obtained within the second excitation type (Figure 4-4). Similar to the first excitation type, the reference case for comparison is the passive control (Figure 4-8).
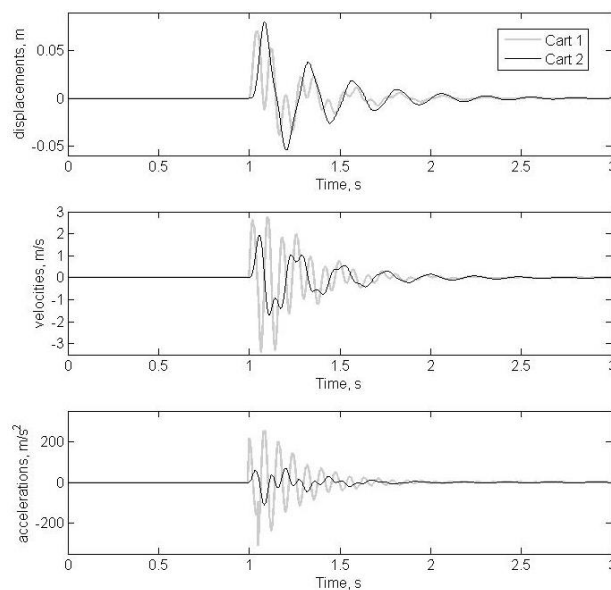

Figure 4-8: Displacements, velocities and accelerations of cart 1 and cart 2 using passive control with the second excitation type

In this case, the relative improvement and the power spectral density results are compared in Figure 4-9 and Figure 4-10, respectively. These Figures show almost the same result as the model with the ramp excitation. The two big differences are as follows: first, the improvement only reaches 4-5% w.r.t the corresponding passive case, so it is much lower than the one obtained in the ramp excitation. Second, the displacement and relative velocity based Groundhook algorithm has the opposite effect in comparison with the ramp excitation.
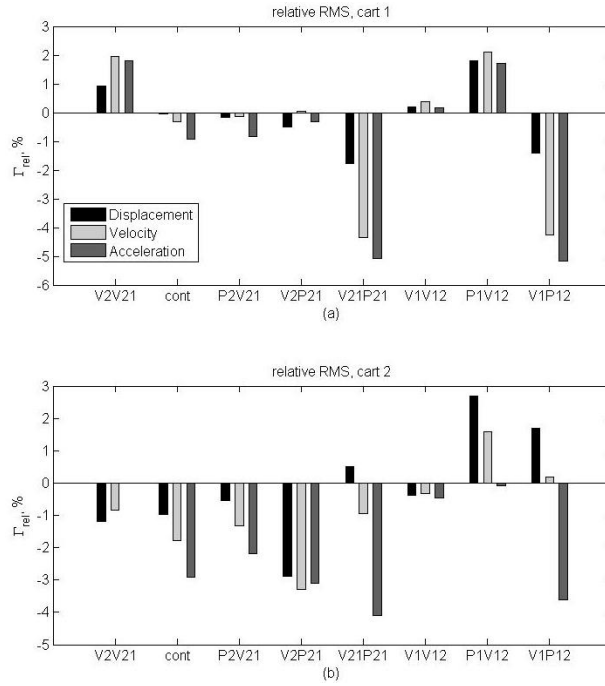

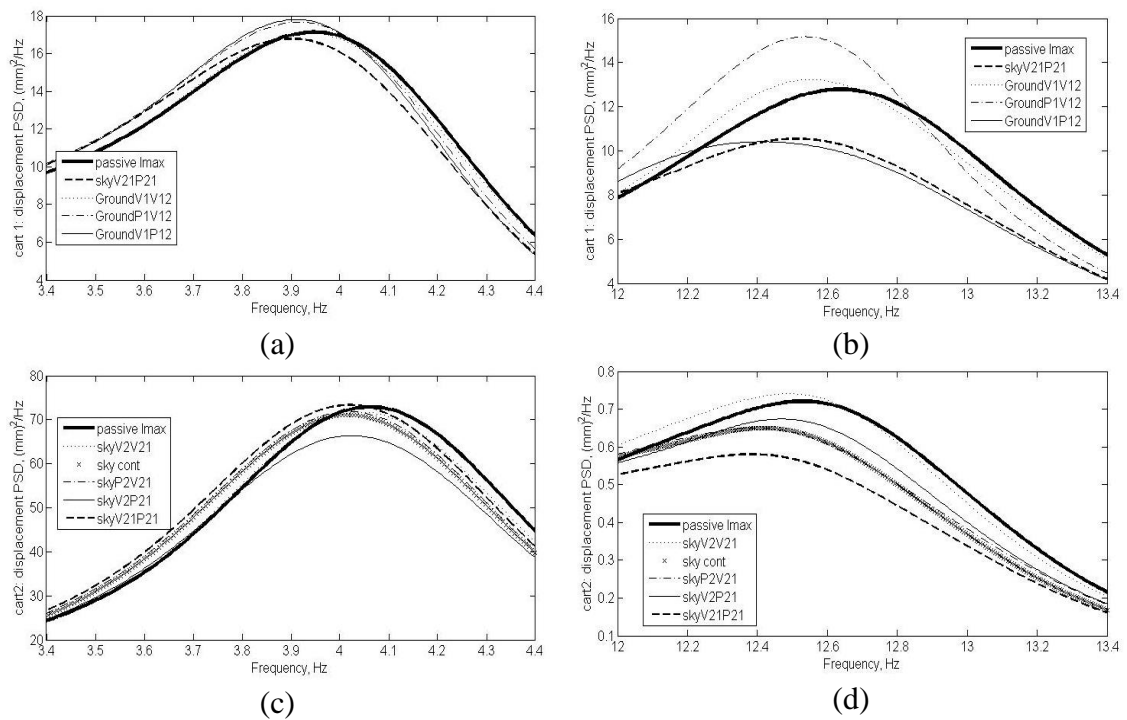Figure 4-9: Improvement of the semi-active control results compare to the passive case in impact excitation

Figure 4-10: Power spectral density for the displacements of the carts under impact excitation

5 LabView Code

In this part, the LabView VI implemented for measurement and vibration control of the two cart test-rig is described. The results attained using the mathematical model (MATLAB code) in the previous section are also verified w.r.t the experimental results to show the applicability of the proposed semi-active vibration control strategies.

5.1 Data acquisition and control system

Before explaining the construction of the LabView code, the data acquisition and control system used in the test-rig are introduced. In addition to the components described in Section 3.1., there are also a data acquisition and a data processing equipment. In this case, the National instruments hardware CompactRIO 9014 and software LabView 2010 are used for data acquisition and processing, respectively. Furthermore, accelerometer and displacement sensors are installed on the test rig to make measurements (Figure 5-1).
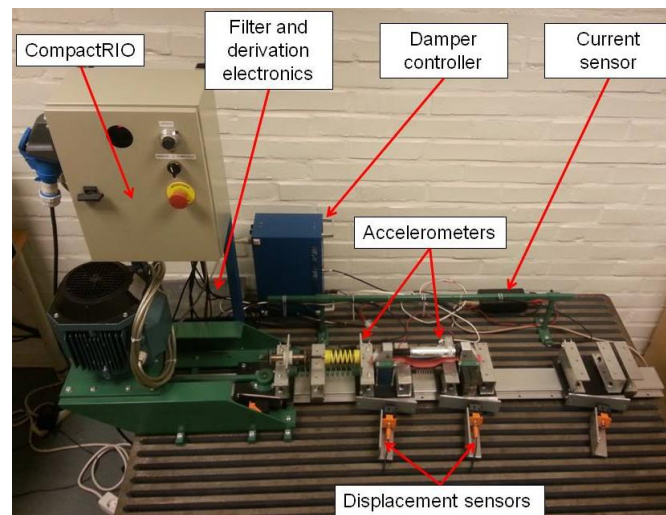
Figure 5-1: Data acquisition and data processing equipment

The CompactRIO controller features an industrial 400 MHz real-time processor for deterministic and reliable real-time (RT) applications. The embedded controller is designed for extreme ruggedness, reliability, and low power consumption that deliver isolated power to the CompactRIO chassis/modules for a 40 to 70 °C operating temperature range [NI, 2013].

The CompactRIO combines:

- ➢ an embedded real-time processor
- ➢ a high-performance FPGA:

Field Programmable Gate Arrays (FPGAs) are programmable semiconductor devices (silicon chips) that are based around a matrix of Configurable Logic Blocks (CLBs) connected through programmable interconnects. FPGAs can be programmed to the desired application or functionality requirements. The FPGA is connected to the embedded real-time processor via a high-speed PCI bus. This represents a low-cost architecture with open access to low-level hardware resources [Xilinx-2013].

> ➢ swappable input/output (I/O) modules:

Each I/O module is connected directly to the FPGA, providing low-level customization of timing and I/O signal processing.

LabView contains built-in data transfer mechanisms to pass data from the I/O modules to the FPGA and also from the FPGA to the embedded processor for real-time analysis, postprocessing, data logging, or communication to a networked host computer such as illustrated in Figure 5-2. The host computer is only used for graphical user interfaces, supervisory control and historical data logging.
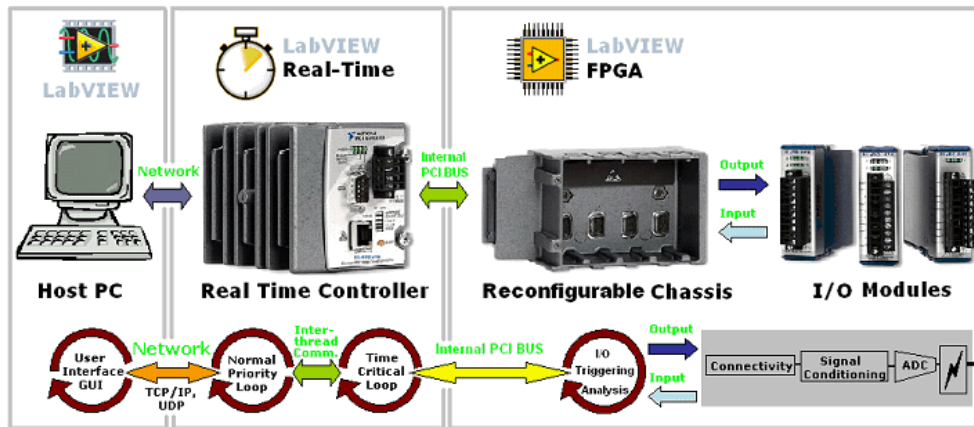

Figure 5-2: CompactRIO Reconfigurable Embedded System Overview [NI, 2013]
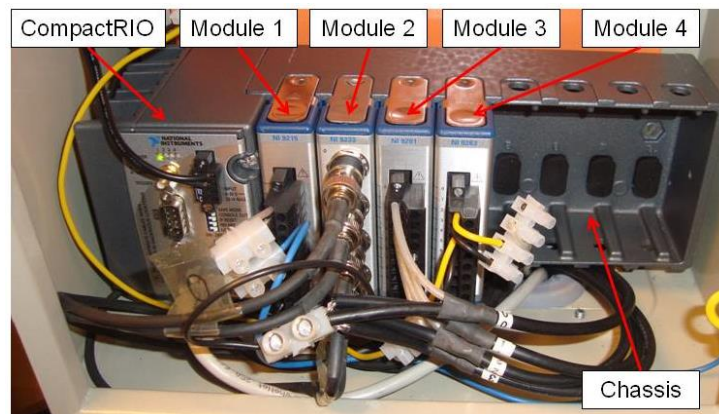
Figure 5-3: CompactRIO with its modules

Four National Instrument I/O modules are added to the CompactRIO (Figure 5-3). The first one is the NI 9215 that gives the value of the damper current measured by a current sensor. Accelerometers are connected to the second module NI 9233 on channels 1 and 2. These accelerometers are produced by IMI Sensors. The model used in our case is the 608A11. The displacement sensors are linked to a filter and derivation electronics in order to calculate velocities of the cars. The displacement sensors are manufactured by IFM. The model of those inductive sensors is the IM5142. Displacements and velocities are collected by the third module NI 9201 on channels 0 to 3. These three modules are analog input modules in contrast with the last one that is an analog output module The NI 9263 module role is to send a control signal to the motor speed controller as well as the MR damper current controller. That current is applied to the MR damper by an electronic circuit called damper controller that can only work in an on-off configuration *i.e.* 0 or 10V, in this case.

5.2 Implementation of the code

There are several tutorials with different levels of complexity available from [NI, 2013] to get started with Labview programming.

As explained before in the National Instrument CompactRIO module, there are two levels of programming: on the FPGA and on the Real-Time processor.

Let's start with the FPGA. The first purpose of this code is to collect data from the sensors and send them to the Real-Time processor. While, the second one is to control the input current that will be sent to the MR damper.

Here is the loop that collects data from sensors (Figure 5-4). As aforementioned, accelerations are given by the module 2 and displacements and velocities are provided by the module 3. Scaling and offset factors should be applied to these raw values, in order to have a smoother data for analysis. Regarding the scaling factors, sensitivity coefficients are written on the calibration certificates that were provided by IMI Sensors at the purchase of each sensor. In contrast, offset factors are not available on these certificates, so additional code is used to calculate the mean value of the noise produced by the sensors when the system is not in service. All these factors are given in Table 5-1.
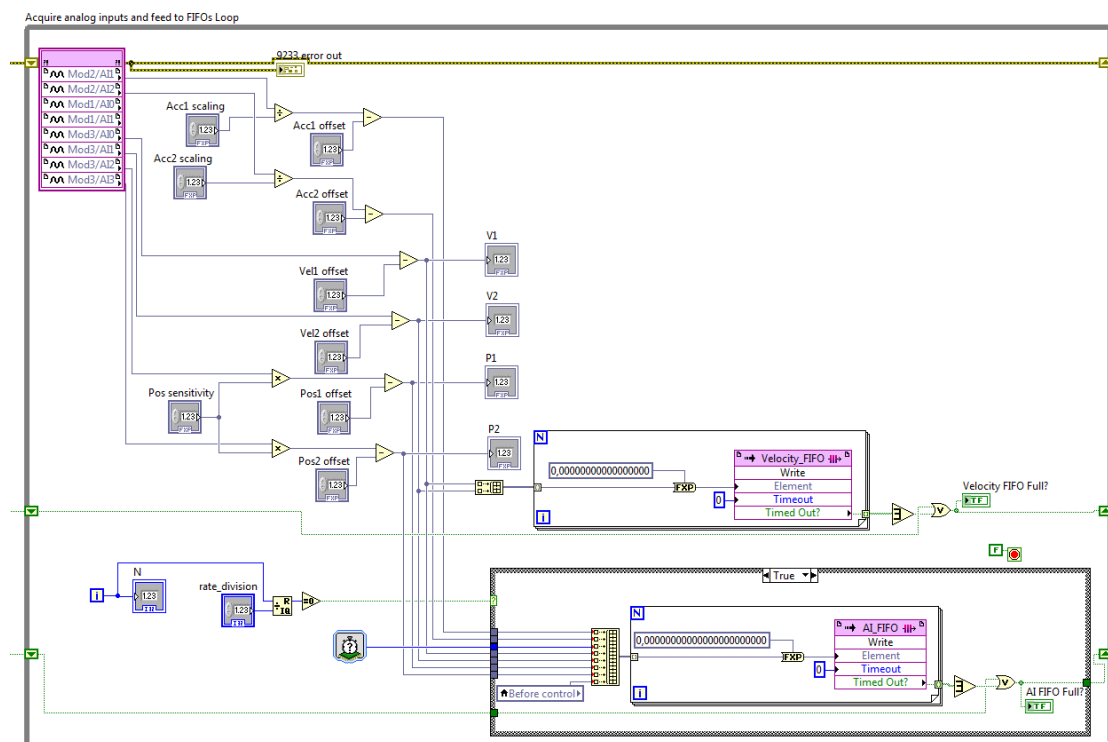

Figure 5-4: Collect data loop

Table 5-1: Sensitivity and offset factors

Parameter	Value
Acceleration 1 sensitivity	0.093 V/g
Acceleration 2 sensitivity	0.104 V/g
Acceleration 1 offset	0.1382 mm/s²
Acceleration 2 offset	0.1133 mm/s²
Displacement 1 sensitivity	0.0184 m/V
Displacement 2 sensitivity	0.0184 m/V
Displacement 1 offset	-0.1375 mm
Displacement 2 offset	-0.1397 mm
Velocity 1 offset	-0.0019 mm/s
Velocity 2 offset	-0.0035 mm/s
Current offset	2.45 A

Once these factors are applied, the resulting data are sent to two buffers so that could be used in the real-time processor. The first buffer, Velocity_FIFO, is used to control the damper current at the real-time level in order to compare the results coming from the FPGA level with the results of the real-time level. The second one, AI_FIFO, is utilized to plot the data and measure the RMS values.

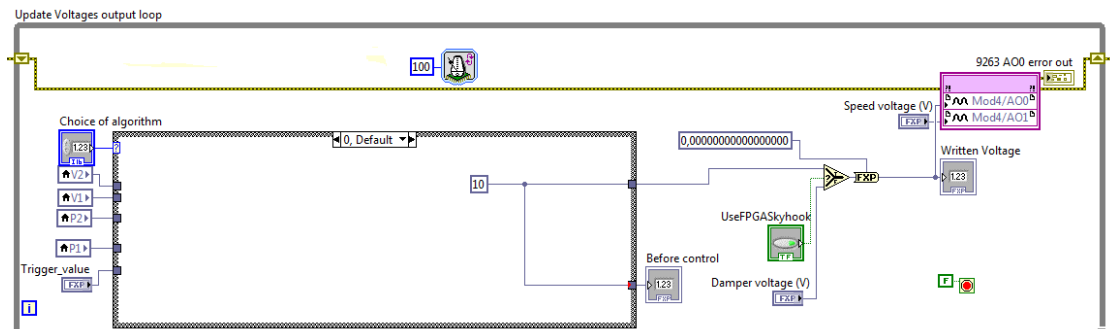The second loop of the FPGA level is shown in Figure 5-5.

Figure 5-5: Control loop on the FPGA

The aim of this loop is to communicate with the output module. So, it controls on one hand the input current to the damper and on the other hand the speed voltage of the motor. The same on-off semi-active control algorithms accomplished in MATLAB code, previously are implemented here in LabView code as well. The only difference here is that instead of comparing the product of the control law, $\dot{x}_2.\dot{x}_{21}$ by example, to zero, it is compared to a trigger value that takes into account the noise produced by the sensors and the lag between $\dot{x}_1$ and $\dot{x}_2$ or x_1 and x_1. In fact, this trigger value acts as a filter and removes the effects of the noise associated with the displacement and velocities of the carts. For each algorithm, an optimized trigger value is determined so that the motions of the cart are the lowest. Beside those semi-active control techniques, two passive cases are configured where 0 or I_{max} can be applied as an input current to the MR damper.

Figure 5-6 (a) and (b) shows the case loop that implements the Skyhook velocity and relative velocity based and the Groundhook displacement and relative velocity based algorithms, respectively.
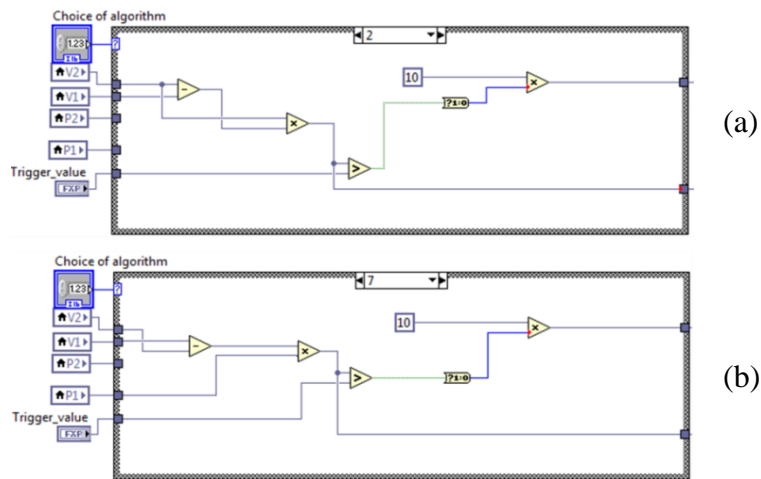
Figure 5-6: Examples of the semi-active control algorithms

The next step is to build the code on the real-time processor.

The first part of this code is dedicated to the motor controller. In order to excite the system in the same way as the ramp defined previously in Section 4.2., a first loop creates a triangular wave signal by specifying how long it takes for the motor to reach the maximum speed (Figure 5-7).
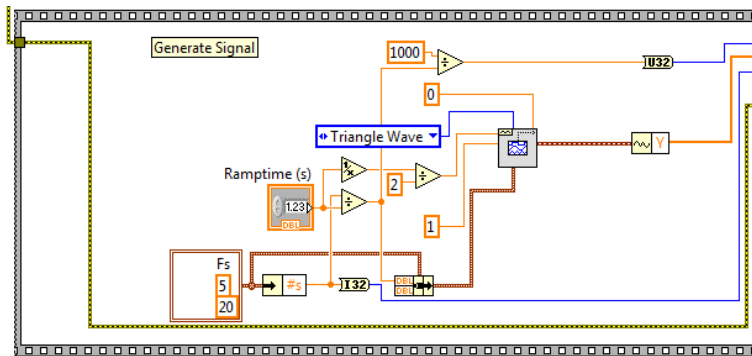
Figure 5-7: First loop of the motor control

Then a second loop (Figure 5-8) is used to specify the maximum velocity that the motor should reach and how many ramps must be performed during the test. There is also a possibility to excite the system at the same frequency by using a manual knop on the motor controller.
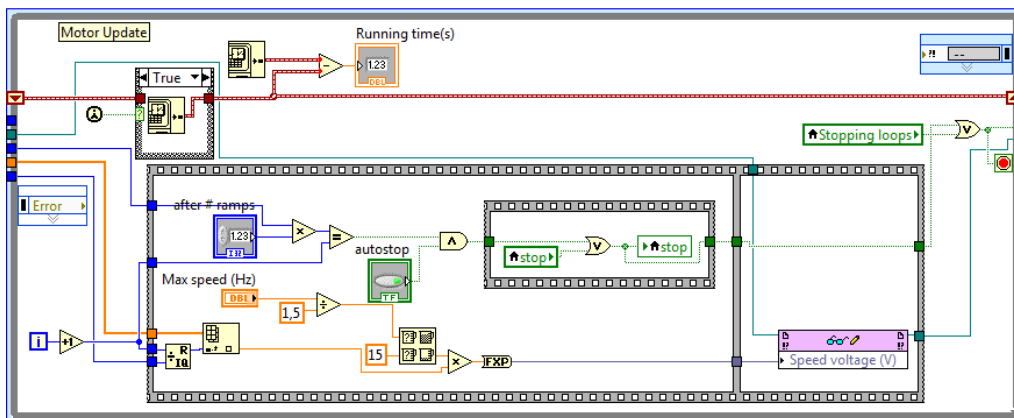
Figure 5-8: Second loop of the motor control

The second part of this level is the control of the current insert in the MR damper (Figure 5-9). This loop includes a case loop that allows applying a filter on the data (coming from the Velocity_FIFO buffer), before control strategies are applied. Another case loop is used for the Skyhook and Groundhook strategies implementation, called Skyhook host and Groundhook host, in order to compare the results obtained by the real-time processor and the FPGA knowing the fact that in the first case a filter is applied while the latter one is much faster. Finally, a third case loop sends the trigger values of all the strategies to the FPGA.
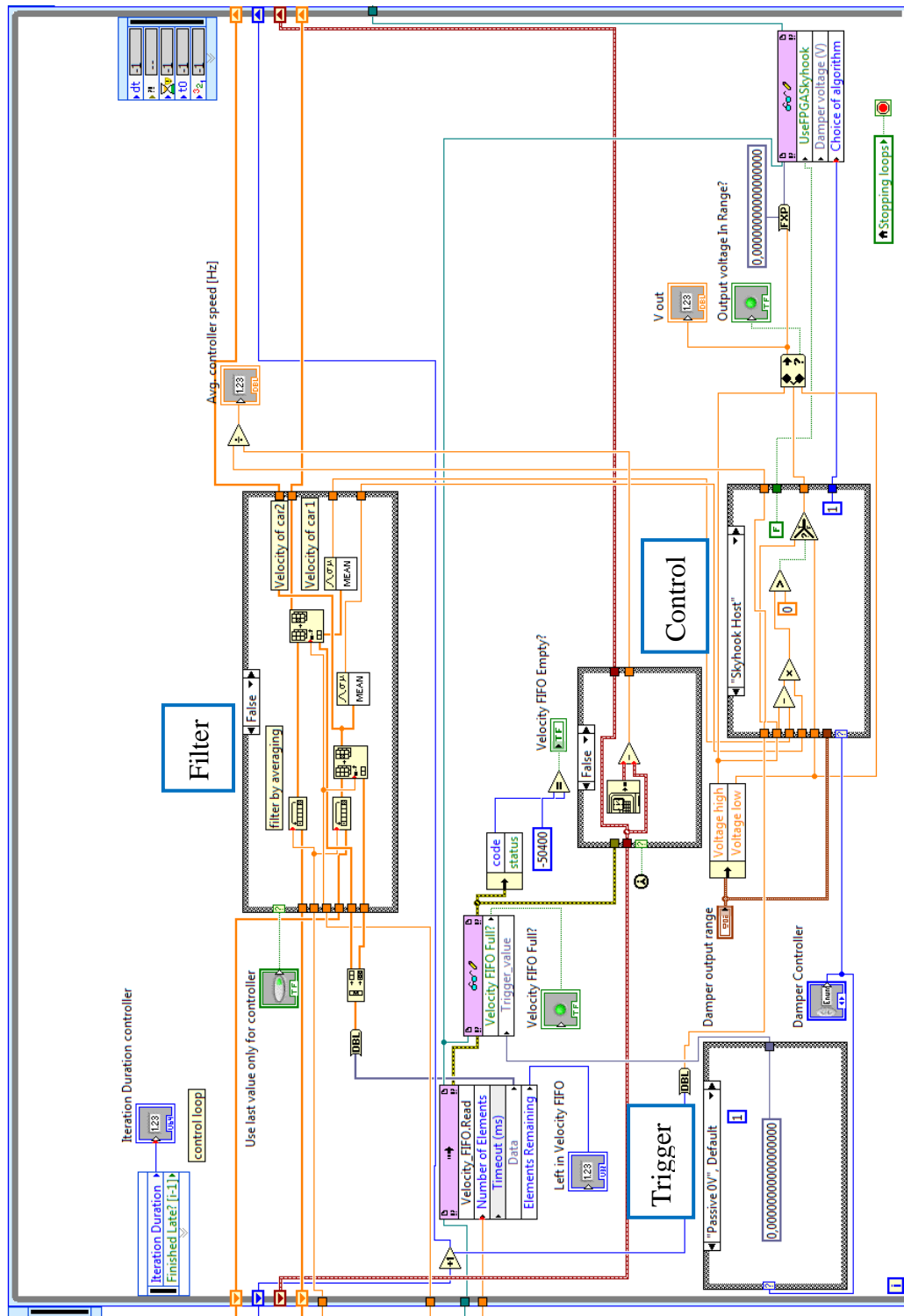
Figure 5-9: Control loop in the real-time processor

The third part of the real-time code is devoted to display the results. The data are first read from the AI_FIFO buffer and 8 arrays are built for containing the 8 types of data, *i.e.* the two displacements, two velocities, two accelerations, also the time and the voltage that are applied to the damper. This procedure is given by the loop shown in Figure 5-10. Then a second loop (Figure 5-11) is created to calculate the RMS and mean values of the two displacements, two velocities and two accelerations corresponding to each cart. Finally, the data are sent to a third loop given in Figure 5-12 to display.
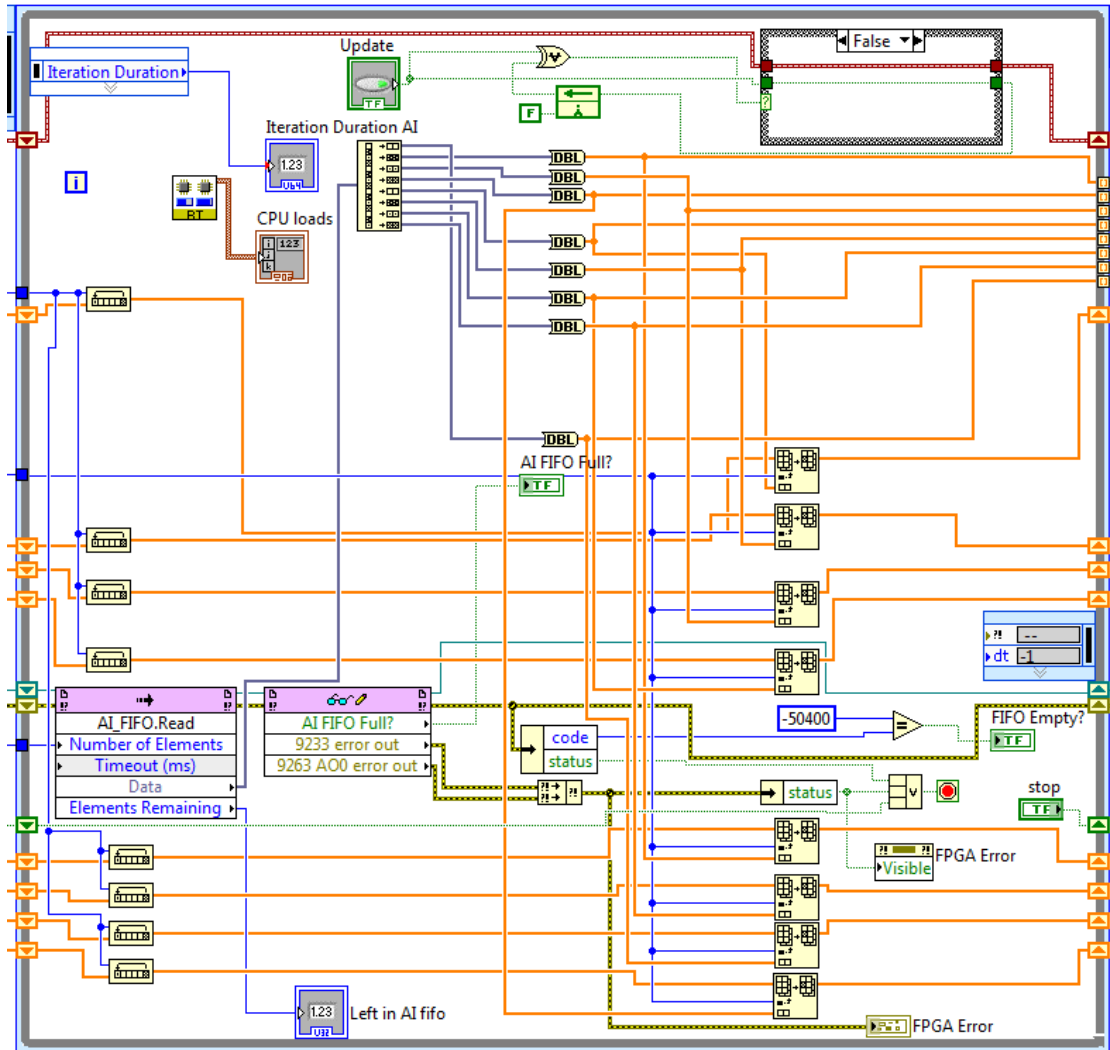
Figure 5-10: Reading data loop
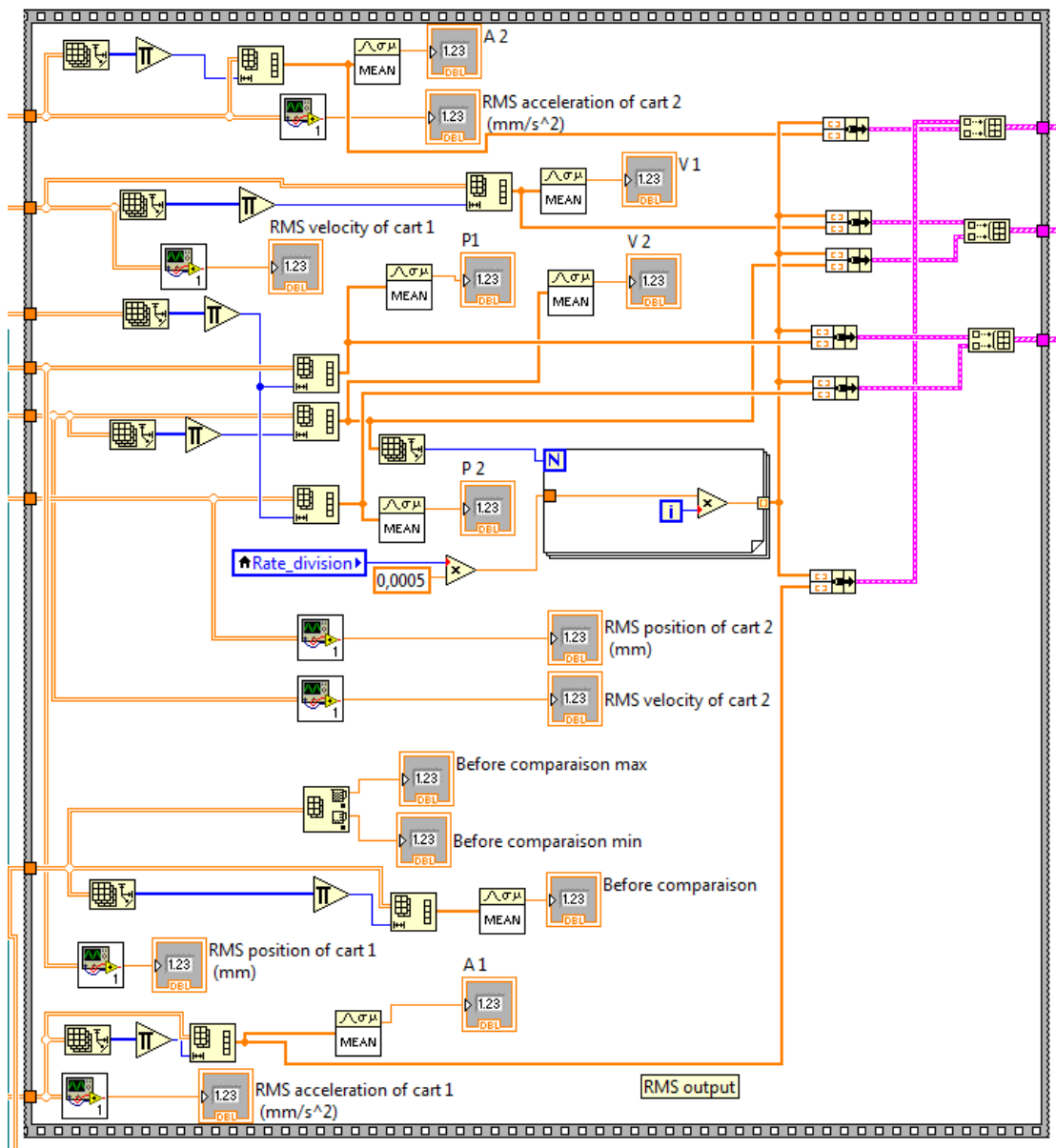
Figure 5-11: Calculating the RMS and mean values loop
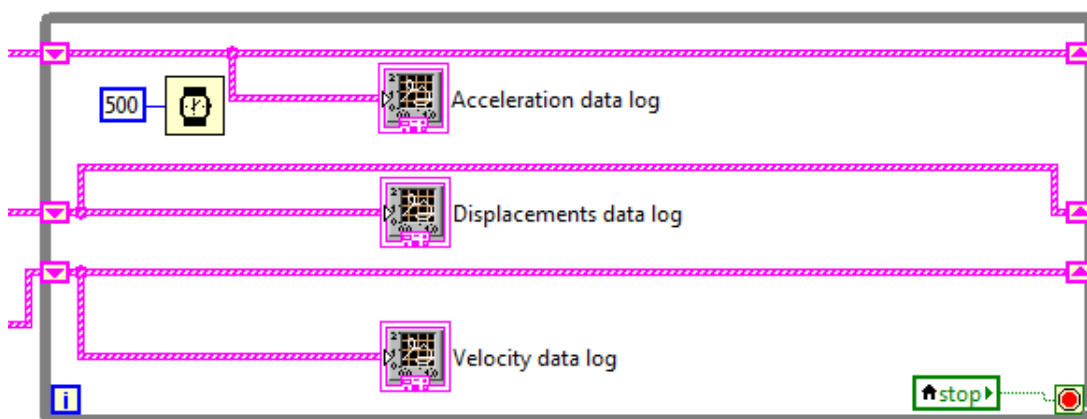
Figure 5-12: Data displaying loop

5.3   Results

It is really necessary to make sure if the existing model for the MR damper and the corresponding parameters are in a good shape or not. Therefore, a deeper investigation on the test rig is performed to check if the MR damper is used in the proper working condition. So measurements are taken to establish the current that is introduced to the MR damper. It turns out that the value of this current is 1.88 A. According to Table 2-1, the allowed continuous input current must be lower than 0.5 A. Thus, once the passive control is used, the input current is almost four times higher than the permitted limit. Consequently, the MR damper input electrical current must be reduced within the admissible range.

It should be noted that the current electric circuit is composed of an alternating voltage source, a switch and a resistor that symbolized the MR damper as shown in Figure 5-13. Several measurements are performed to determine all these unknown properties and the results are gathered in Table 5-2.
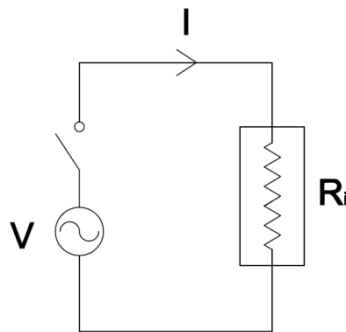
Figure 5-13: Schematic representation of the current electric circuit

Table 5-2: Properties of the system

Parameter	Value
The voltage of the source V	33.8 V
The intern resistance of the MR damper R_i	18 Ohm
The current going through the system I	$I = \dfrac{V}{R_i} = \dfrac{33.8}{18} = 1.88\ A$

In order to decrease the input current and bring it to the admissible range, an easy solution could be to put a resistor in series together with the MR damper. The series case shown in Figure 5-14 represents this idea. In this case, the total resistance can be found as the sum of the circuit resistances given by equation (5-1).
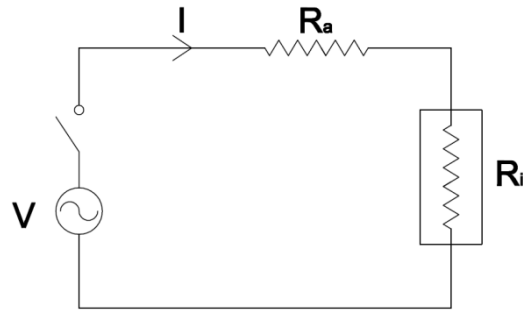
Figure 5-14: Schematic representation of the series resistance case

$$R_{tot} = R_i + R_a \tag{5-1}$$

The optimized current has to be close and beneath 0.5 A according to Section 4.3. Therefore, equation (5-2) has to be solved in order to determine the lowest resistor R_a that should be added to the system:

$$R_{tot} = R_i + R_a = \frac{V}{I} \tag{5-2}$$

Rearranging this equation leads to:

$$R_a = -R_i + \frac{V}{I} = -18 + \frac{33.8}{0.5} = 49.6 \, Ohm \tag{5-3}$$

This means that, the additional resistor must be higher than 49.6 Ohm. Therefore, a resistor of 54.4 Ohm is built and is introduced to the system to decrease the electrical input current to the MR damper from 1.88 A to 0.47 A (which is within the design admissible range).

Once this modification is completed the experiments can be repeated. Initially, the excitation sweeps a frequency range from 0 to 14 Hz and then gets back to 0 Hz in order to cover both Eigenfrequencys of the system. But now, it appears that the MR damper does not introduce a sufficient force in the system. Indeed, when the second Eigenfrequency is going to be reached, the two carts start to collide. As a result, another modification on the test rig has to be accomplished to the excitation at this stage. The maximum frequency that can be reached without the carts collision is 10 Hz. The frequency of the motor follows the same trend as the ramp implement in the mathematical model.

From statistical point of view, increasing the number of ramps can improve the results' reliability. Therefore, the reference case is chosen as the ramp shown in Figure 4-3 that is applied three times consecutively. It should be noted that the passive control is applied using the maximum current, *i.e.* 0.47 A. The results of this case are given in Figures 5-15 to 5-17 which show displacements, velocities and accelerations of both carts, respectively.

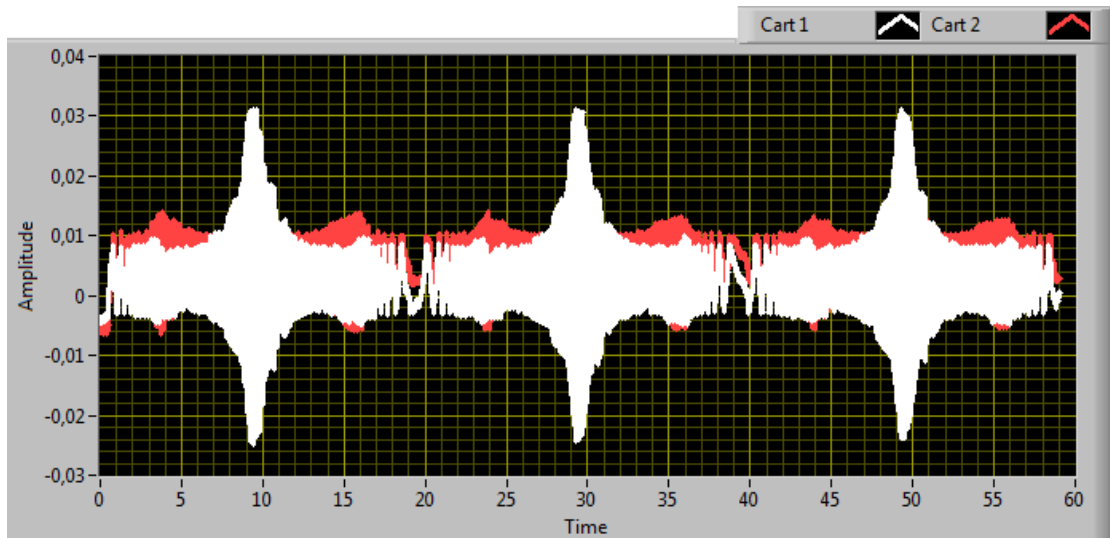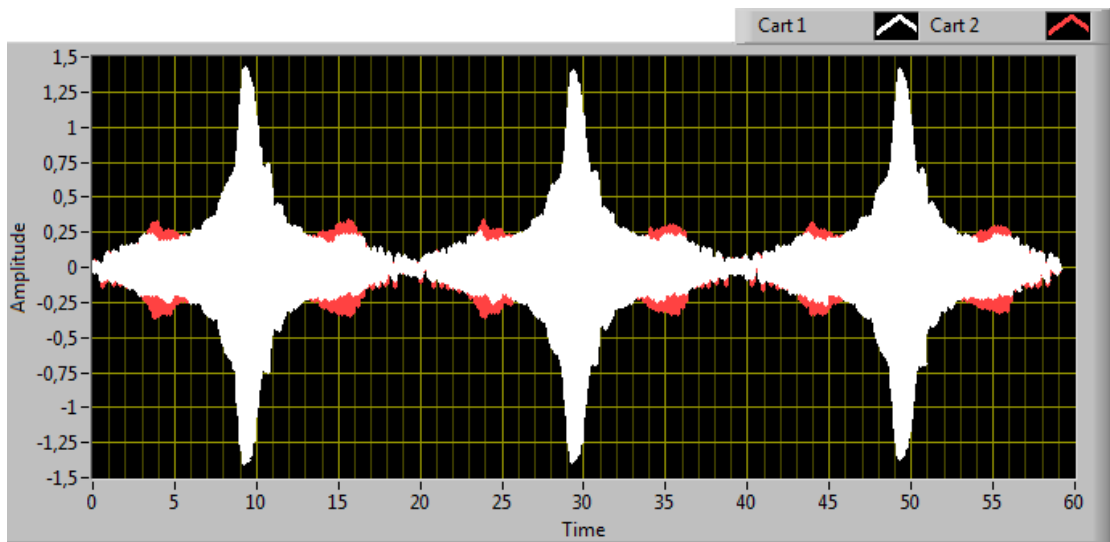*Figure 5-15: Displacement of cart 1 and 2 in meter*

Figure 5-16: Velocities of cart 1 and 2 in m/s
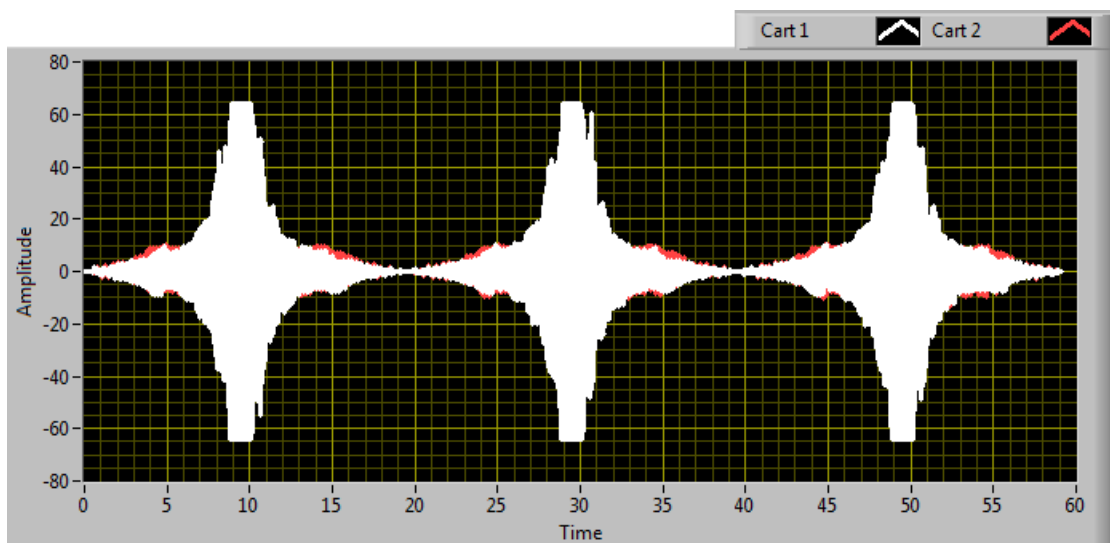
Figure 5-17: Accelerations of cart 1 and 2 in m/s²

It is really difficult to compare the materials given in those time domain graphs. So the RMS value of positions, velocities and accelerations are calculated and compared for each cart. The Table 5-3 sums up these values.

Table 5-3: RMS values for the passive control

	Position (m)	Velocity (m/s)	Acceleration (m/s²)
Cart 1	0,00695	0,2958	16,3668
Cart 2	0,00661	0,1654	7,37323

The same experiments are performed for all the semi-active control strategies implemented in the LabView code (in addition to the two strategies implemented in the real-time processor). The results are presented in Table 5-4.

Table 5-4: RMS values results of all the strategies

	Position (m)		Velocity (m/s)		Acceleration (m/s²)	
Strategy	Cart 1	Cart2	Cart 1	Cart2	Cart 1	Cart2
Sky host	0.00693	0.00658	0.2823	0.1470	15.6017	7.0990
Ground host	0.00679	0.00656	0.2766	0.1530	15.3700	7.1509
V2V21	0.00684	0.00639	0.2780	0.1482	15.3763	7.0909
P2V21	0.00673	0.00650	0.2728	0.1471	15.2345	6.9910
V2P21	0.00678	0.00626	0.2739	0.1406	15.1967	6.8843
V21P21	0.00669	0.00631	0.2684	0.1387	15.0931	6.8469
V1V12	0.00692	0.00673	0.2810	0.1471	15.5560	7.1818
P1V12	0.00675	0.00674	0.2702	0.1449	15.1325	6.9655
V1P12	0.00673	0.00680	0.2695	0.1439	15.1093	6.9247

In order to have a better representation of the results, the improvements associated with each of the strategies are calculated in the same way as discussed earlier in equation (4-19).

Figure 5-18 resumes the results of various studied cases. Different control strategies implemented are given in the x-axis, while the y-axis represents the improvement w.r.t. the passive control in percentage. Part (a) of this graph shows the results for the cart 1 and part (b) exhibit the results for the cart 2.
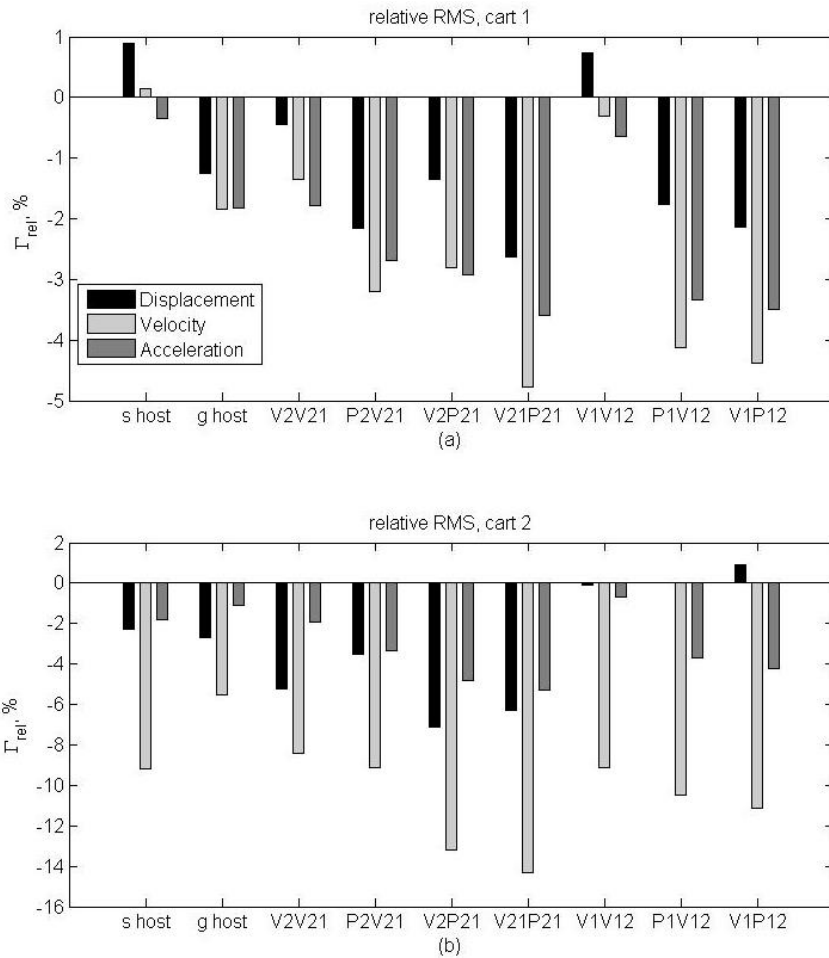
Figure 5-18: Vibration control improvement using the semi-active control strategies compare to the passive one

It follows that; first the strategies implemented on the real-time processor and on the FPGA are compared. For the Skyhook on the real-time (s host in the graph), the results are in good agreement with the theory. This means that vibrations of cart 1 are slightly increased while the vibrations of cart 2 are reduced. However, that is not the same as the case for the control law implemented on the FPGA level (V2V21 on the graph). Indeed vibrations of both carts are mitigated in this case but there is more improvement on displacement and acceleration of cart 2. Regarding the Groundhook laws, g host and V1V12, they don't show the expected behaviour. Instead of decreasing the motion of cart 1 and increasing the motion of cart 2, both Groundhook policies decrease both carts. But this is the same conduct as the simulations run on MATLAB.

It can be deduced that the two best algorithms for vibration reduction of cart 1 are the control strategies based on the relative velocity and the relative displacement (V21P21) as well as the Groundhook law based on the velocity and the relative displacement based (V1P12). Consequently, if the purpose is to minimize the vibration of cart 2, the most two efficient algorithms are the Skyhook control based on the relative velocity and the relative displacement (V21P21) and the Skyhook control based on the velocity and the relative displacement (V2P21).

5.4 Verification

In this section, experimental results are compared with those obtained mathematically using MATLAB.

Foremost, absolute RMS values are considered. From Figures 4-9 and 5-18 it can be concluded that the results are in the same magnitude order. Indeed, displacements are of the order of centimetres, velocities are of the order of decimetres per second and accelerations are of the order of decametres per square second in Figures 4-5 and 5-15 to 5-17. But it appears that there is a scaling factor ranging from 1.3 to 4 between experimental and theoretical values. That might be due to the fact that the damping coefficients between the cart and the track may not be estimated in a proper way. Another explanation is that in MATLAB code the model used to simulate the MR damper force is the Bouc-Wen model but there is a modified Bouc-Wen model according to the literature which might reduce the modelling errors. In total, modelling and measurement errors might be the reason behind such differences between the theoretical and experimental results.

Furthermore, regarding the improvement provided by both theoretical and experimental cases, they both yield the same conclusion as follows: the best two algorithms for vibration suppression in the first and second carts are respectively the semi-active control based on the velocity and the relative displacement V1P12 and V2P21. However, the semi-active case based on the relative velocity and relative displacements (V21P21) gives satisfactory results for vibration reduction in both carts, simultaneously (according to the theoretical and experimental results).

As expected, the experiment results do not yield the same improvement as the ideal case attained from MATLAB simulations. In addition to the modelling and measurement errors, another reason of this outcome might be due to the fact that there is always some time delay in the test rig between the time that the current control signal is send and the time that the MR damper respond to that change. More importantly, that the MR damper components properties including the MR fluid are subject to change due to time, different working conditions and so on. In our case and before the aforementioned modifications applied to the MR damper input current, the damper was subject to higher electrical loads than the admissible design range. That might affect the performance of the MR damper coil, negatively and influence the results.

6   Conclusion

The purpose of this chapter is to summarize the work that is done for this Master thesis. In addition, the results of testing will be discussed with respect to the research objectives set. The chapter ends with recommendations for future work in the field of semi-active vibration dynamics control.

6.1 Summary

In this thesis, application of Magneto-Rheological (MR) dampers in semi-active vibration dynamics control of a multi-cart system has been studied. The dynamics and vibration behaviour of a two cart system have been investigated mathematically and a similar experimental test-rig has been employed to verify the theoretical results. The purpose of this Master thesis was to investigate the efficiency of several semi-active control strategies (regarding the vibration isolation) with respect to the corresponding passive case and select the most efficient algorithms.

First, the multi-cart system has been modelled in MATLAB and the Bouc-Wen theory has been utilized to represent the mathematical behaviour of the MR damper. Different types of semi-active control strategies as well as passive vibration control technique have been implemented through the MATLAB code. The system dynamics response also the RMS values at the displacement, velocity and acceleration levels of the carts have been analysed. In each case the results have been compared to the corresponding optimized passive control for vibration suppression of the sprung and unsprung masses while two types of base excitations have been applied. Through these simulations, the expected benefits of Skyhook control have been confirmed.

Afterwards, five on-off alternative control strategies including two for the Skyhook, two for the Groundhook and one that is common for both, together with a continuous Skyhook algorithm have also been implemented and compared. It turned out that all of them were showing advantageous than the regular Skyhook and Groundhook laws. These results have been achieved for the two excitation types. However, only the displacement and relative velocity based Groundhook algorithms exhibits brilliant results for the frequency ramp excitation. As a summary, the two best algorithms for vibration reduction of cart 1 are the semi-active control based on the relative velocity and the relative displacement (V21P21) and the Groundhook law based on the velocity and the relative displacement (V1P12). At least to the author's search the latest one has not been considered as a Groundhook strategy however it provides really promising results according to the simulations and experiments. On the other hand, if the purpose is to minimize the vibration of cart 2, the two most effective algorithms are the semi-active control based on the relative velocity and the relative displacement (V21P21) and the Skyhook control based on the velocity and the relative displacement (V2P21).

In the next step, the passive and semi-active strategies explored earlier have been implemented, experimentally through a LabView VI. In order to measure and analyse the data from the experimental test-rig using LabView, two levels of programming have been considered (real time and FPGA). During the experiments, only the frequency range excitation has been applied and on-off strategies have been implemented due to the limitation of the hardware of the test rig.

The outcome of the experimental part was in agreement with theoretical analysis. That means that the best algorithms introduced earlier for the mathematical model have

shown the best results for the experimental test-rig as well. However, there were some deviations in the theoretical and experimental results that might be due to the modelling and measurement errors also MR damper working condition.

6.2 Future work

The first work that could be done in this field is to determine the precise values of the damping coefficient between the carts and the track, so that the mathematical model get closer as much as possible to the experimental test rig values. In addition, the modified Bouc-Wen or Spencer models (presented in Appendix B), can be implemented for modelling the MR damper in as much as it shows better accuracy than the Bouc-Wen model.

An extension to this work would be to extend the assessments of each semi-active control algorithm by applying other base excitations. Another interesting point would be to compare the energy consumption of each strategy to determine the one that is the most effective in terms of vibration isolation and energy consummation.

As shown in the mathematical model, an on-off and a continuous Skyhook strategies using the same algorithm are implemented. That means that both of them decide which input current is chosen by using the velocity and relative velocity based algorithm (V2V21). It appears that this continuous strategy is four to five times more effective than the on-off strategy. So another study can be conducted to see if the continuous strategy based on the relative velocity and the relative displacement (V21P21) by example shows the same benefits compared to the on-off strategy. This algorithm can be written as:

$$I = \begin{cases} I_{cont} & if \ \dot{x}_{21}.x_{21} \geq 0 \\ I_{off} & if \ \dot{x}_{21}.x_{21} < 0 \end{cases} \tag{6-1}$$

Where I_{cont} is given by :

$$\min_{I_{cont} \in [I_{off}, I_{on}]} (F(I_{cont}) - F_{sky}) \tag{6-2}$$

Within the frame of the existing experimental hardware, only zero current, as I_{off}, or maximum of current, as I_{on}, can be introduced to the MR damper. Several researches have been performed based on a value different from zero as I_{off}. It would be interesting to compare the results obtained with a value slightly greater than zero with the results acquired using zero as I_{off}. Although to achieve this goal, the experimental hardware has to be changed.

Due to the same reason, only on-off strategies were investigated during this thesis. Indeed, with this device only I_{off} or I_{on} can be introduced to the MR damper. During library researches, not only on-off semi-active strategies were found, also continuous semi-active and active strategies can be implemented. In fact the damper current controller should be active or semi-active to be able to provide the desired input current to the MR damper. Solving this problem might give the possibility to explore active vibration control strategies such as LQR method or the continuous Skyhook control. In order to manage that, it requires again to do some modifications to the hardware so that not only I_{off} or I_{on} are inserted but also values in between. By example, an adjustable current source or a rheostat has to be installed so that the input current can be adjusted in real-time.

7 References

Ahmadkhanlou, F. (2008): *Design, Modeling and Control of Magnetorheological Fluid-Based Force Feedback Dampers for Telerobotic Systems*. Ph.D. Thesis. The Ohio State University, Columbus, OH.

BASF Co. (2009): Badische Anilin- und Soda-Fabrik, http://www.basf.com.

Ben Mekki, O. (2006): *Amortissement Semi-Actif Des Structures Flexibles.* Ph.D. Thesis. Ingegneria Delle Strutture e Geotecnica Dell'universita Di Roma, Tor Vergata, Italy, 213 pp..

Berbyuk, V. (2010): *Vibration Dynamics and Control*, Department of Applied Mechanics, Chalmers University of Technology, Göteborg, Sweden, 225 pp.

Berbyuk, V. (2012): *Vibration Dynamics and Control*, Department of Applied Mechanics, Chalmers University of Technology, Göteborg, Sweden, 273 pp.

Carlson, J. D. (2002): What makes a good MR fluid?. *Journal of Intelligent Material Systems and Structures*, Vol. 13, No. 7, pp. 431–436.

Cavey, R. H. (2008): *Design and Development of a Squeeze-Mode Rheometer for Evaluating Magneto-Rheological Fluids*. Ph.D. Thesis. Department Of Mechanical Engineering, Virginia Polytechnic Institute and State University, Blacksburg, Virginia, USA, 156 pp.

Delphi Corporation (2009): http://www.delphi.com.

Demersseman, R. (2009): *Caractérisation et modélisation causale d'un frein à liquide magnétorhéologique en vue de sa commande*. Ph.D. Thesis. Département de génie électrique, Ecole Nationale Supérieurs d'Arts et Métiers, Paris, France, 169 pp.

Félix-Herrán, L., Mehdi, D., Soto, R., Rodríguez-Ortiz, J. de J., and Ramírez-Mendoza, R. A. (2010): *Control of a semi-active suspension with a magnetorheological damper modeled via Takagi-Sugeno*. 18th Mediterranean Conference on Control & Automation, Congress Palace Hotel, Marrakech, Morocco, 23-25 June 2010, pp.1265-1270.

Goncalves, F. D. (2001): *Dynamic Analysis of Semi-Active Control Techniques for Vehicle Applications*. Ph.D. Thesis. Department of Mechanical Engineering, Virginia Polytechnic Institute and State University, Blacksburg, Virginia, USA, 195 pp.

Hadadian, A. (2011): *Optimal Design of Magnetorheological Dampers Constrained in a Specific Volume Using Response Surface Method*. Ph.D. Thesis. Department of Mechanical and Industrial Engineering, Concordia University, Montreal, Quebec, Canada, 139 pp.

Hoyle, A., Arzanpour, S., and Shen, Y. (2010): A Novel Magnetorheological Damper Based Parallel Planar Manipulator Design. *Smart Materials and Structures* 19: (05)5028, 9 pp.

Karnopp, D., Crosby, M. J., and Harwood, R. A. (1974): Vibration control using semi-active force generators. *Journal of Engineering for Industry*, Vol. 96, No. 2, pp. 619–626.

Koo, J. H. (2003): *Using Magneto-Rheological Dampers in Semi-active Tuned Vibration Absorbers to Control Structural Vibrations.* Ph.D. Thesis. Department of

Mechanical Engineering, Virginia Polytechnic Institute and State University, Blacksburg, Virginia, USA, 160 pp.

Li, W. H., Yao, G. Z., Chen, G., Yeo, S. H., and Yap, F. F. (2000): *Testing and steady state modeling of a linear MR damper under sinusoidal loading.* Mechanics of Machines Lab, School of Mechanical & Production Engineering, Nanyang Technological University, Singapore, 9 pp.

Lord Corporation (2009): http://www.lord.com.

Lozada, J. (2007): *Modélisation, contrôle haptique et nouvelles réalisations de claviers musicaux.* Ph.D. Thesis. Department of Mechanic, Ecole Polytechnique, Paris, France, 187 pp.

Metered, H. A. (2010): *Modelling and control of magnetorheological dampers for vehicle suspension systems.* Ph.D. Thesis. School of Mechanical, Aerospace and Civil Engineering, University of Manchester, 220 pp.

Motech Biedermann Co. (2009): http://www.biedermann.com.

National Intruments (2013): http://www.ni.com

Nguyen, Q. H., and Choi, S. B. (2009): *Optimal design of MR shock absorber and application to vehicle suspension.* Department of Mechanical Engineering, Inha University, Incheon, Korea, 11 pp.

Nygårds, T. (2001): *Washing Machine Design Optimization Based on Dynamics Modeling*, Ph.D. Thesis. Department of Applied Mechanics, Chalmers University of Technology, Göteborg, Sweden, 197 pp.

Nygårds, T., and Berbyuk V. (2012): *Multibody Modeling and Vibration Dynamics Analysis of Washing Machines*, Multibody System Dynamics, 27, 197-238 pp.

Nyman, P., Olason, A., Olsson, M., Pedersen, J., Westman, J., and Östling, G. (2008): *Modellering av Magnetreologisk Friktionsdämpare.* Bachelor Thesis. Department of Applied Mechanics, Chalmers University of Technology, Göteborg, Sweden, 53 pp.

Phulé, P. P. (2001): Magnetorheological (MR) fluids: Principles and applications. *Smart Materials Bulletin*, Vol. 2001,No. 2, pp.7–10.

Poynor, C. P. (2001): *Innovative Designs for Magneto-Rheological Dampers.* Ph.D. Thesis. Department of Mechanical Engineering, Virginia Polytechnic Institute and State University, Blacksburg, Virginia, USA, 88 pp.

Rabinow, J. (1948): The magnetic fluid clutch. *Transactions of the American Institute of Electrical Engineers*, Vol. 67, No. 2, pp. 1308–1315.

Rakheja, S., and Sankar, S. (1985): Vibration and shock isolation performance of a semi-active on-off damper. *Journal of Vibration, Acoustics, Stress, and Reliability in Design*, 107(4), pp. 398-403.

Sapiński, B., and Filuś, J. (2003): *Analysis of Parametric Models of MR Linear Damper.* Department of Process Control, University of Mining and Metallurgy, Warsaw, Poland, 26 pp.

Sleiman, H. (2010): *Systèmes de Suspension Semi-Active à Base de Fluide Magnétorhéologique pour l'Automobile.* Ph.D. Thesis. Département de Génie Électrique, École Nationale Supérieure d'Arts et Métiers, Paris, France, 202 pp.

Song, X., Ahmadian, M., and Southward, C. (2005): Modeling *m*agnetorheological *d*ampers *w*ith *a*pplication *o*f *n*onparametric *a*pproach. *Journal* o*f Intelligent Material Systems* a*nd Structures*, Vol. 16, 13 pp.

Spencer Jr., B. F., Dyke, S. J., Sain, M. K., and Carlson, J. D. (1996): Phenomenological Model of a Magnetorheological Damper. *ASCE Journal of Engineering Mechanic*, 23 pp.

Wang, J., Meng, N., Feng, N., and Hahn, E. J. (2005): *Dynamics* Performance and control of squeeze mode MR fluid damper–rotor system. *Smart Materials and Structures*, Vol. 14, pp. 529–539.

Wen, Y. K. (1976): Method for random vibration of hysteretic systems. *ASCE Journal of the Engineering Mechanics Division*, 102(2): pp. 249-263.

Xilinx Incoeporation (2013): www.xilinx.com

Yoshioka, H., Ramallo, J., and Spencer Jr., B. (2002): Smart Base Isolation Strategies Employing Magnetorheological Dampers. *American Society of Civil Engineers*, pp. 540-551.

Zhu, X., Jing, X., and Cheng, L. (2012): *Magnetorheological fluid dampers: A review on structure design and analysis.* Department of Mechanical Engineering, The Hong Kong Polytechnic University, Hung Hom, Kowloon, Hong Kong, China, 35 pp.

8 Appendix

8.1 Appendix A:

MR fluid operational modes

The three common MR fluid operational modes include valve, shear, and squeeze modes. A summary on these is done by [Biedermann, 2009], [Cavey, 2008], [Demersseman, 2009] and [Wang, 2005].

Those modes are briefly described as follows:

➢ Valve mode:

The valve mode is the most common one among the three operational modes for MR fluids and serves as the primary method used in MR dampers.

In this mode, MR fluid flows between fixed magnetic poles. This means that it flows perpendicular to the magnetic flux lines and thus perpendicular to the ferrous particle chains as well as shown in Figure (8-1). The flow of MR fluid in the valve mode is also referred to as the pressure driven flow mode as described by Lord Materials Division.
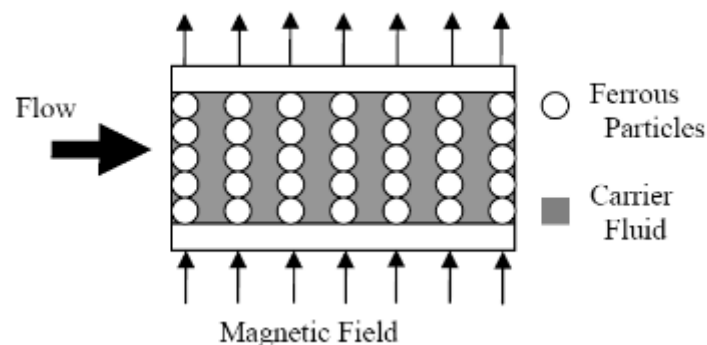

Figure 8-1: MR fluid in valve mode with an applied magnetic field [Cavey, 2008]

In the valve mode operation, a magnetic field is applied across a fluid gap, forming ferrous particle chains in the fluid. As the fluid flows through this device, it continuously breaks and then nearly instantaneously reforms the ferrous particle chains. Varying the intensity of the applied magnetic field changes the strength of these chains and in turn the apparent viscosity of the MR fluid. In the valve mode, there is a pressure drop across the fluid as it flows through the device. This pressure drop is essentially what is used in different devices, such as shock absorbers, to resist an input force.

➢ Shear mode:

In the shear mode (also referred as direct shear mode), the MR fluid experiences a relative shearing force from one of the plates enclosing the fluid gap. Ferrous particle chains (as shown in Figure 8-2) are formed along the flux path of the magnetic field, which runs perpendicular to the pole plates just the same as in the valve mode configuration. What separates the shear mode from the valve mode is that the pole plates are not stationary in this case. Indeed, one of the pole plates moves parallel with respect to the other one which causes a shearing force to develop across the fluid gap. Just as in the valve mode operation, ferrous particle chains form a mechanical resistance to fluid flow in response to an applied magnetic field. The intensity of the applied magnetic field determines the apparent viscosity of the MR fluid and thus the force transmitted between the pole plates. This mode is the second most common kind of MR fluid operation and is used for some shock absorbers, clutches and brakes.
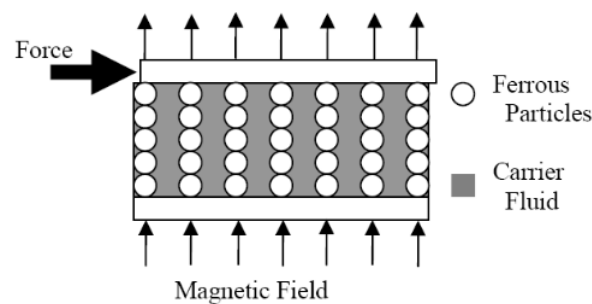

Figure 8-2: MR fluid in shear mode with an applied magnetic field [Cavey, 2008]

➢ Squeeze mode:

The squeeze mode uses a layer of fluid in the order of millimetre disposed between two moving surfaces in an orthogonal direction to the fluid and traversed by a magnetic field (Figure 8-3). It is thought that this mode effectively places the ferrous particle chains in a situation similar to columnar buckling. As with the other modes of operation, the strength of the ferrous particle chains is dependent on the intensity of the applied magnetic field. However, unlike the other modes, the usable force generated from squeeze mode is not due to an increase in apparent viscosity. Typically, in the squeeze mode devices there is a little or even no flow of MR fluid. The force supported is a mechanical property of the ferrous particle chains rather than the apparent viscosity change of the fluid. This mode can be found in applications with low amplitudes such as certain vibration isolators.
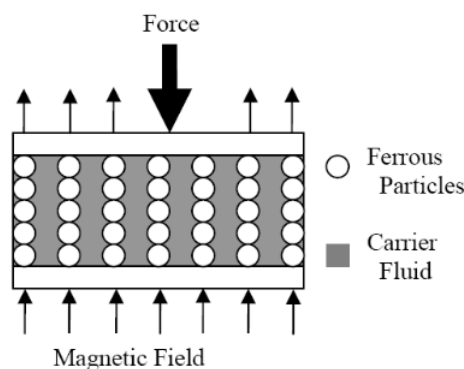

Figure 8-3: MR fluid in the squeeze mode setup prior to axial force with an applied magnetic field [Cavey, 2008]

8.2 Appendix B:

Comparison of the model of MR damper

In order to analyse the different models, identification experiments are undertaken by [Spencer, 1996]. The aim was to designate the parameter values for these models that are necessary for simulation.

> ➤ The Bingham model:

The idealization of the visco-plastic MR damper model uses similarities in the rheological behaviour of the electro-rheological (ER) and the MR fluids and employs the similar techniques in the modelling of ER dampers.

In the rheological structure shown in Figure (8-4), in which the Bingham model is considered as a base, there is a Coulomb friction element f_c placed parallel to the dashpot c_0. According to the Bingham's MR damper model proposed by [Spencer, 1996], for non-zero piston velocities (), the damping force F can be expressed as equation (8-1)

$$F = f_c.sgn\,\dot{x} + c_0.\dot{x} + f_0 \tag{8-1}$$

Where f_c is the frictional force, c_0 is the viscous damping parameter and f_0 is the force due to the presence of the accumulator. This last simplification in the model results from the assumption that the elasticity which represents the accumulator activity has a low stiffness and linear characteristics.
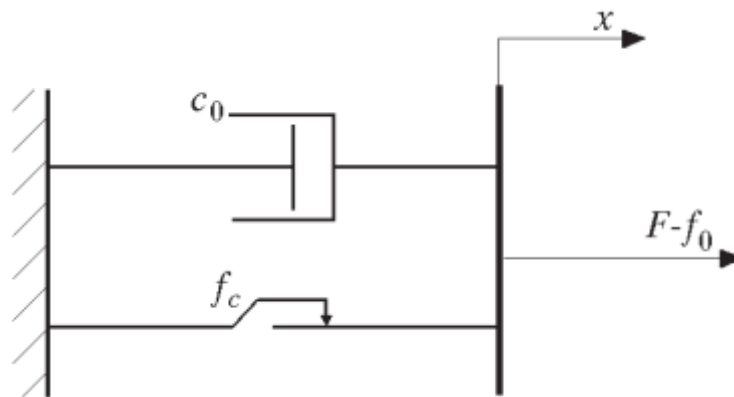

Figure 8-4: Rheological structure containing a friction and dashpot element to simulate Bingham's model of a MR fluid damper [Sapiński, 2003]

According to [Spencer, 1996], this model cannot correctly simulate the operation of the damper at low speeds as shown in Figure 8-5. In fact, this model does not take into account the presence of hysteresis between back and forth phases. In addition, the change in slope between low speeds and higher speeds is not perfectly reproduced by the Bingham model.
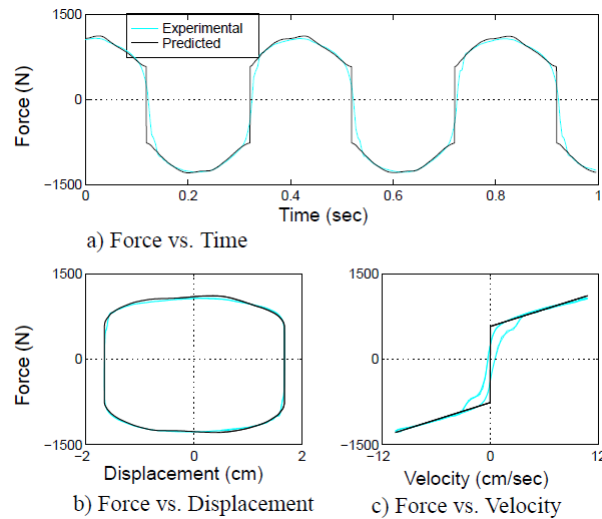
a) Force vs. Time

b) Force vs. Displacement   c) Force vs. Velocity

Figure 8-5: Comparison between the predicted and experimentally obtained responses for the Bingham model [Spencer, 1996]

➢ The modified Bingham plastic model or the Gamota-Filisko model:

An extension of the Bingham MR damper model is the visco-elasto-plastic model formulated by Gamota and Filisko [Spencer, 1996]. This extension depends on the connection of the Bingham, Kelvin-Voight body and the Hooke body models (Figure 8-6). The Kelvin-Voight model represents a solid body, whose maximum elongation exclusively depends on the applied force (independent of time).

Characteristic for this model is the appearance of the creeping phenomenon (elongation gradually increases as a result of the delayed damper activity). The Hooke's model, in turn, for which the spring elongation is proportional to the applied force and independent of time, represents the ideal elastic body. The damping force in the Gamota-Filisko model (see Figure 8-6) can be described as equation (8-2).

$$F = \begin{cases} \begin{cases} k_1(x_2 - x_1) + c_1(\dot{x}_2 - \dot{x}_1) + f_0 \\ \quad = c_0\dot{x}_1 + f_c.sgn\,(\dot{x}_1) + f_0 \quad if \quad |F| > f_c \\ \quad = k_2(x_3 - x_2) + f_0 \end{cases} \\ \begin{cases} k_1(x_2 - x_1) + c_1\dot{x}_2 + f_0 \\ \quad = k_2(x_3 - x_2) + f_0 \end{cases} \quad if \quad |F| \le f_c \end{cases} \qquad (8\text{-}2)$$

Where,

- c_0, f_0, f_c are the parameters representing the viscous damping, force due to the presence of the accumulator and frictional force (Bingham model), respectively.
- k_1, c_1 represent the stiffness and damping of the body (Kelvin-Voigt model), respectively.
- k_2 is the stiffness of the elastic body (Hooke model).

It should be noted that when $|F| \le f_c$, then $\dot{x}_1 = 0$, which means that once the friction force f_c related to the new stress in the fluid is greater than the damping force F the piston remains motionless.
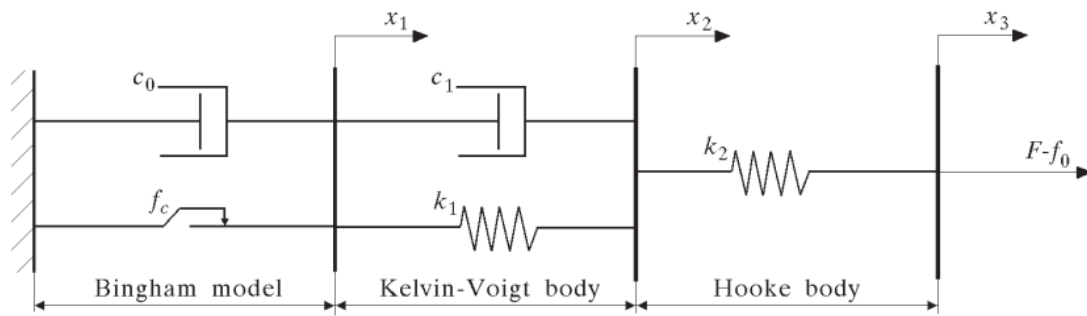
Figure 8-6: Rheological structure of a MR damper for the Gamota-Filisko model [Sapiński, 2003]

A comparison between the predicted responses and the corresponding experimental data is provided in Figure (8-7). As expected, this model can portray the force-displacement behaviour of the damper in a well manner. In addition, it possesses the force-velocity behaviour that more accurately resembles the experimental data. The hysteresis phenomenon is well visible. However, this model does not reproduce a satisfactory behaviour at low velocities and since the governing equations (3), (4) are extremely stiff, making them difficult to deal with numerically.
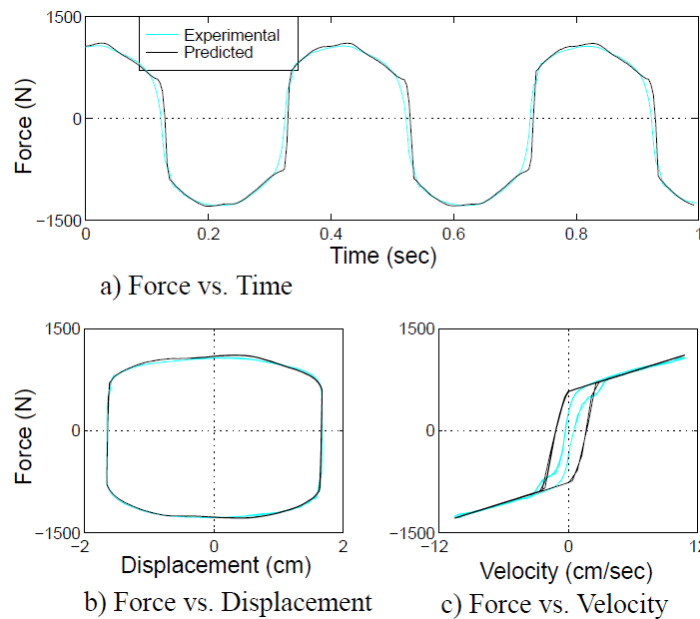

a) Force vs. Time

b) Force vs. Displacement

c) Force vs. Velocity

Figure 8-7: Comparison between the predicted and experimentally obtained responses for the Gamota-Filisko model [Spencer, 1996]

➢ The Li model:

Another view of the visco-elasto-plastic properties of MR fluids in the modelling of MR damper behaviour is the model proposed by [Li, 2000]. This model is divided into two areas; pre and post-yield. In these areas the MR fluid shows visco-elastic and visco-plastic body properties, respectively. This conforms to the rheological structures presented in Figure 8-8.
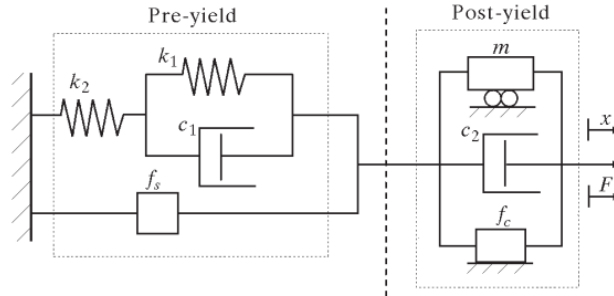

Figure 8-8: Rheological structure of a MR damper for the Li model [Li, 2000]

Li proposed a description of a MR fluid state in the pre-yield area of a visco-elastic model, in which a Hooke's body (spring k_2) is in series with a KelvinVoight's body (spring k_1 and dashpot c_1). Besides the visco-elastic force f_{ve}, a contribution to the damping force in the pre-yield area also carries the static friction force f_s, resulting from the type of seal applied in the damper. Accordingly, the damping force F in the pre-yield area can be written as equation (8-3).

$$F = f_{ve} + f_s \qquad (8\text{-}3)$$

Where the force f_{ve} is described by the equation (8-4):

$$\dot{f}_{ve} + \frac{k_1 + k_2}{c_1} f_{ve} = \frac{k_1 . k_2}{c_1} x + k_2 \dot{x} \qquad (8\text{-}4)$$

Where, the damping force F crosses the plastic flow force f_c (when $\tau \geq \tau_y(H)$), once the damper operates in the post-yield area. Then damping force is also equal to the visco-plastic force, in which, besides the friction force connected with the fluid shear stress f_c, the viscotic force and inertial force contribute. This can be written as equation (8-5)

$$F = f_c . sgn\, \dot{x} + c_2 \dot{x} + m\ddot{x} \qquad (8\text{-}5)$$

Where c_2 is a co-factor of the viscotic friction, and m is the mass of replaced MR fluid dependent on the amplitude and frequency of a kinematic excitation applied to the piston. As such, the damping force in the Li model is expressed as equation (8-6):

$$F = \begin{cases} f_{ve} + f_s & if\ |F| \leq f_c \\ f_c . sgn\, \dot{x} + c_2 \dot{x} + m\ddot{x} & if\ |F| > f_c \end{cases} \qquad (8\text{-}6)$$

A comparison between the predicted responses and the corresponding experimental data is provided in Figure (8-9). The graphs show the reconstructed force versus displacement as well as force versus velocity hysteresis cycles compared with the practical experimental curves. It can be seen from the plots that the model can predict

the experimental data very well. Also, it seems that the inertial effect plays no obvious role in this case (f =1.0 Hz), which can be reflected from Figure ???. However, when the frequency is above 4.0 Hz, the inertial effect cannot be ignored. A mathematical model, which can accurately reflect the higher frequencies under the effect of damping force, still needs further study.
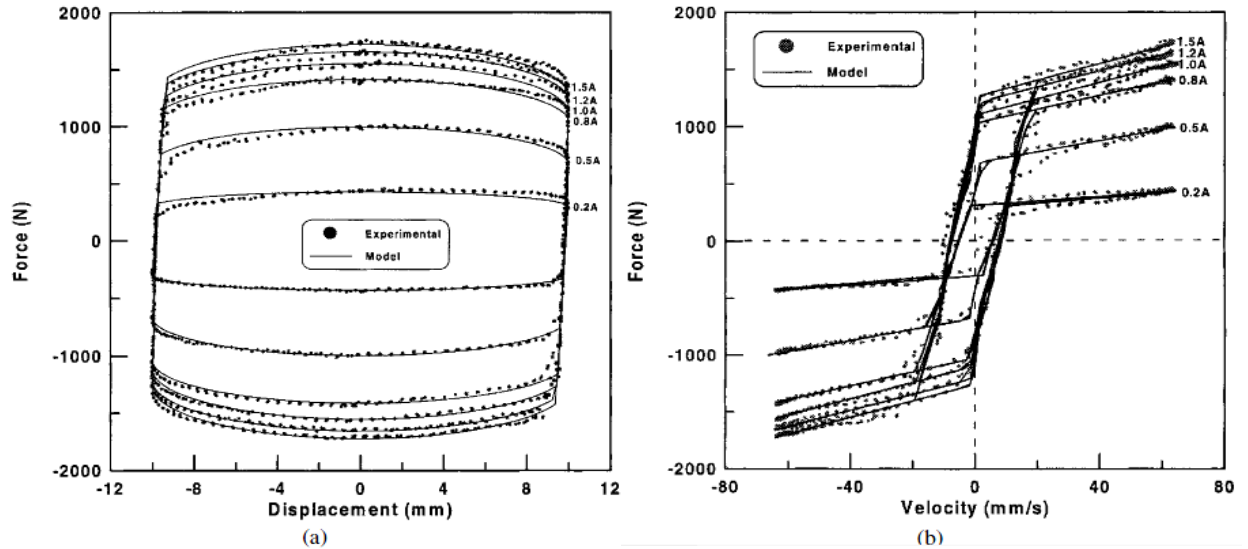

Figure 8-9: Comparison between the predicted and experimentally obtained response for the Li model [Li, 2000]

➤ The Bouc-Wen model:

This model has been previously presented in Section 2.1.2.2., but it is numerically tractable and has been proposed to account for the hysteresis behaviour at low speed.

➤ The modified Bouc-Wen model or Spencer model:

To better predict the damper response in the region where the acceleration and velocity have opposite signs and the velocities are small, a modified version of the Bouc-Wen model is proposed by [Spencer, 1996], as shown in Figure 8-10. This model consists of a Bouc-Wen model in series with a damper having damping parameter c_1 and in parallel with a spring having stiffness k_1. Parameter c_1 takes care of MR damper behavior when velocity is around zero. Nominal damper force is determined by the spring stiffness k_1.
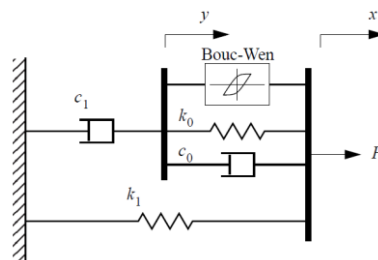

Figure 8-10: Rheological structure of a MR damper for the Spencer model [Sapiński, 2003]

To obtain the governing equations for this model, consider only the upper section of the model. The forces on either sides of the rigid bar are equivalent. Therefore,

$$c_1 \dot{y} = \alpha z + k_0(x - y) + c_0(\dot{x} - \dot{y}) \tag{8-7}$$

where, the evolutionary variable z is governed by equation (8-8)

$$\dot{z} = -\gamma |\dot{x} - \dot{y}||z|^{n-1}z - \beta(\dot{x} - \dot{y})|z|^n + A(\dot{x} - \dot{y}) \tag{8-8}$$

Solving equation (8-7) for $\dot{y}$ results in

$$\dot{y} = \frac{1}{c_0 + c_1}[\alpha z + c_0\dot{x} + k_0(x - y)] \tag{8-9}$$

The total force generated by the system is then found by summing up the forces in the upper and lower sections of the system in Figure 8-10 yields

$$F = \alpha z + c_0(\dot{x} - \dot{y}) + k_0(x - y) + k_1(x - x_0) \tag{8-10}$$

Inserting equation (8-7) into equation (8-10), the total force can be rewritten as equation (8-11)

$$F = c_1\dot{y} + k_1(x - x_0) \tag{8-11}$$

A comparison between the predicted responses and the corresponding experimental data is provided in Figure 8-11. The proposed model for the damper predicts the behaviour of the MR damper very well in all regions, including the region where the acceleration and velocity have opposite signs and the magnitude of the velocities are small.
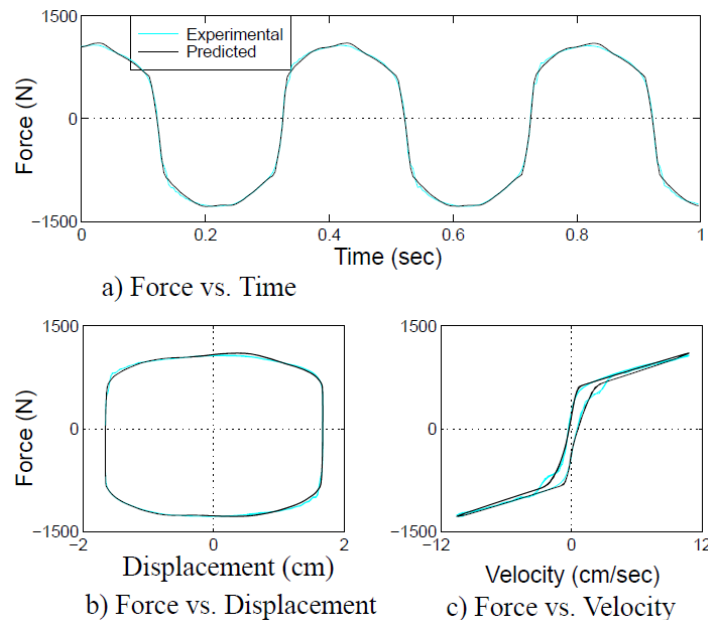

a) Force vs. Time

b) Force vs. Displacement   c) Force vs. Velocity

Figure 8-11: Comparison between the predicted and experimentally obtained response for the Spencer model [Spencer, 1996]

➢ Non-parametric model

The non-parametric model consists of a series of functions that can follow the experimental data from a MR damper. The first step is to interpret and examine data from experiments to find the patterns that can recreate the equations. For example, the hysteresis is described by a hyperbolic tangent (tanh) function.

The model proposed by [Song, 2005] is composed of the following functions:

1) A polynomial function: A function such as equation (8-12) is used to describe the maximum damping force as a function of the applied current.

$$A_{mr}(I) = \sum_{i=0}^{n} a_i I^i \qquad (8\text{-}12)$$

Where, A_{mr} is the maximum damping force, a_i is the polynomial coefficients with appropriate units, n is the order of the polynomial, and I is the current applied to the MR damper.

2) A shape function: Several functions proposed below are used to preserve the resulted wave-shape correlation between the damper force and relative velocity across the damper, also represent the bilinear behavior of the force–velocity curve.

$$S_b(\dot{x}) = tanh[(b_1 I + b_0)\dot{x}] \qquad (8\text{-}13)$$

$$S_b(\dot{x}) = sgn(\dot{x})\left[1 - exp\left(\frac{-(b_0|\dot{x}|)}{\dot{x}_0}\right)\right] \qquad (8\text{-}14)$$

$$S_b(\dot{x}) = \frac{(b_0 + b_1|\dot{x} - \dot{x}_0|)^{b_2(\dot{x}-\dot{x}_0)} - (b_0 + b_1|\dot{x} - \dot{x}_0|)^{-b_2(\dot{x}-\dot{x}_0)}}{b_0^{b_2(\dot{x}-\dot{x}_0)} + b_0^{-b_2(\dot{x}-\dot{x}_0)}} \qquad (8\text{-}15)$$

In equation (8-15), $b_0 > 1$, $b_1 > 0$ and $b_2 > 0$ are constants, $\dot{x}$ is the velocity across the MR damper and $\dot{x}_0$ is a constant. Since $tanh$ is an exponential based function, it has been observed that equation (8-13) is too flat to describe the force–velocity bending curve at the large velocity region. Thus, equation (8-13) is modified as equation (8-15) to avoid such modelling discrepancy. Combining equations (8-12) and one of equations (8-13), (8-14) or (8-15) yields the damper force as a function of the damper current and relative velocity, i.e.,

$$F_s = A_{mr}(I)S_b(\dot{x}) \qquad (8\text{-}16)$$

3) A delay function: A first-order filter is used to create the hysteresis loop. In the state space form, this filter is formulated as

$$\dot{y} = -(h_0 + h_1 I + h_2 I^2)y + h_3 F_s \qquad (8\text{-}17)$$

$$F_h = (h_0 + h_1 I + h_2 I^2)y + h_4 F_s \qquad (8\text{-}18)$$

Where, y is a state variable of the filter, $h_i, i = 0 - 4$, are constants, and I is the input current applied to the MR damper

4) <u>An offset function:</u> In some cases, the damping force is not centered at zero because of the gascharged accumulator effect in the damper. Therefore, it is necessary to include a force bias in the model, such as equation (8-19):

$$F_{mr} = F_h + F_{off} \qquad (8\text{-}19)$$

where, F_{off} represents the nonzero centered damping force mainly resulting from the accumulator, and F_{mr} is the MR damping force.

8.3 Appendix C:

Different types of MR Dampers

Four technologies are generally used to design the MR dampers. Geometry, size and performance of each type are specific with respect to the application domain.

➢ Sponge-type MR fluid damper is introduced in Section 3.2.

➢ Mono Tube MR Dampers, described as follows:

It is kind of shock absorber which is the most commonly used according to [Metered, 2010]. The geometry comprises a single tube containing the fluid, the piston and its rod, and a reservoir of pressurized gas at the foot of the shock absorber body (Figure 8-12). It is commonly used in the car seat suspension.

The gas chamber or accumulator contains a compressed gas (usually Nitrogen) and its floating piston provides a slightly moveable barrier between the MR fluid and the gas. The accumulator serves three purposes:

- It provides a degree of softening by providing an extra allowance for the volume changes that occur when the piston rod enters the housing.

- It accommodates thermal expansion of the fluid.

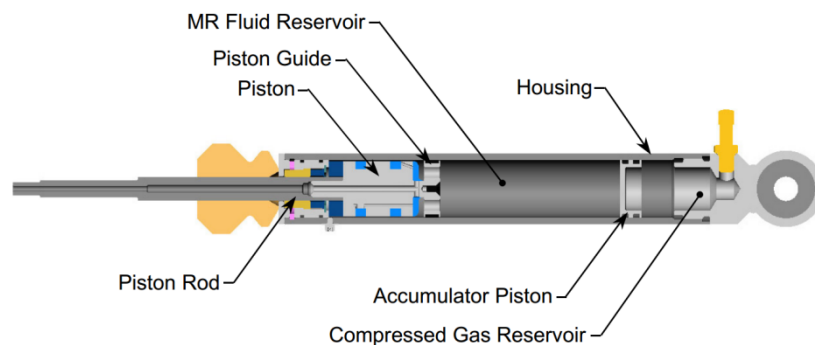- It prevents cavitation in the MR fluid during piston movements.

Figure 8-12: Schematic configuration of the MR shock absorber [Nguyen, 2009]

In this configuration two operation modes are possible. In the first case, the magnetic circuit is entirely contained in the piston (see Figure 8-13 (a)). The gap is machined inside the piston and the space located between the piston and the cylinder is blocked by a seal. The device operates in a valve mode only. The flow is established due to a pressure difference of MR fluid chambers located on either sides of the piston. In the second case (shown in Figure 8-13 (b)) the magnetic circuit is mobile and the air gap between the moving piston and the body of the damper serves here to guide the magnetic flux. The damper operates simultaneously in valve mode due to the pressure difference on either sides of the piston and shear mode due to the relative movement of the piston with respect to the cylinder.
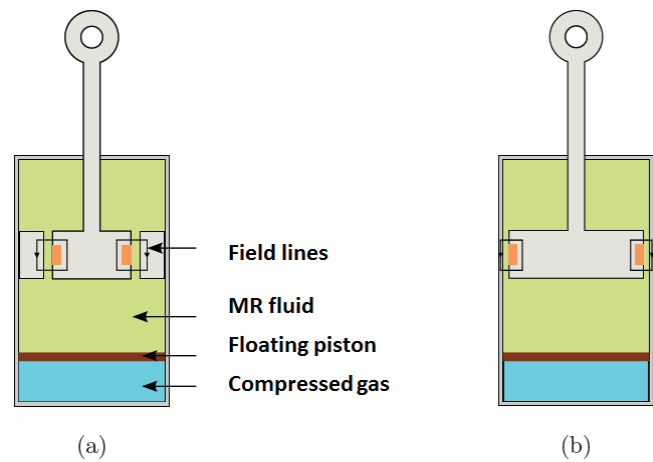
Field lines

MR fluid

Floating piston

Compressed gas

(a)   (b)

Figure 8-13: Geometries of a mono tube damper operating in (a) valve mode and (b) in valve and shear modes [Sleiman, 2010]

➢ A twin tube MR damper

The twin tube MR damper, presented by [Koo, 2003], has two fluid reservoirs, one inside of the other, as shown in Figure 8-14. In this configuration, the damper has an inner and outer housing. The piston rod assembly is guided by the inner housing, in precisely the same way as in a mono tube damper. The volume included in the inner housing is the inner reservoir; the outer reservoir is the volume that is enclosed by the space between the inner housing and the outer housing. The inner reservoir is full of MR fluid so that no air bubbles exist.

An outer reservoir that is partly full of MR fluid helps to accommodate variations in volume due to piston rod motion. Therefore, the outer tube in a twin tube damper serves the same objective as the pneumatic accumulator mechanism in a mono tube damper. In practice, a valve assembly, or a "foot valve," is fastened to the bottom of the inner housing to control the flow of fluid between the two reservoirs. As the piston rod enters the damper, MR fluid flows from the inner reservoir into the outer reservoir through the compression valve, which is part of the foot valve assembly. The amount of fluid that streams from the inner reservoir into the outer reservoir is identical to the volume moved by the piston rod as it enters the inner housing.
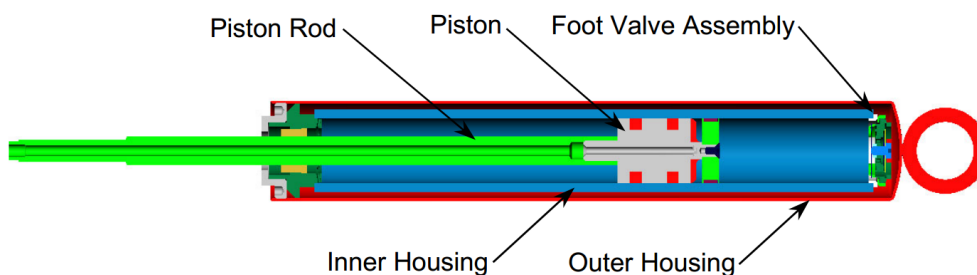

Piston Rod   Piston   Foot Valve Assembly

Inner Housing   Outer Housing

Figure 8-14: Schematic configuration of the twin tube MR damper [Poynor, 2001]

➢ Double-ended MR damper

This type of damper has a piston rod of equal diameter that protrudes from both ends of the damper housing. Figure 8-15 shows a cross-sectional view of a typical double-ended MR damper. Since there is no change in volume as the piston rod moves with respect to the damper body, the double-ended damper does not require an accumulator mechanism. Double-ended MR dampers have been used for bicycle applications, gun recoil applications, and for controlling building sway motion caused by wind gusts and earthquakes [Poynor, 2001].
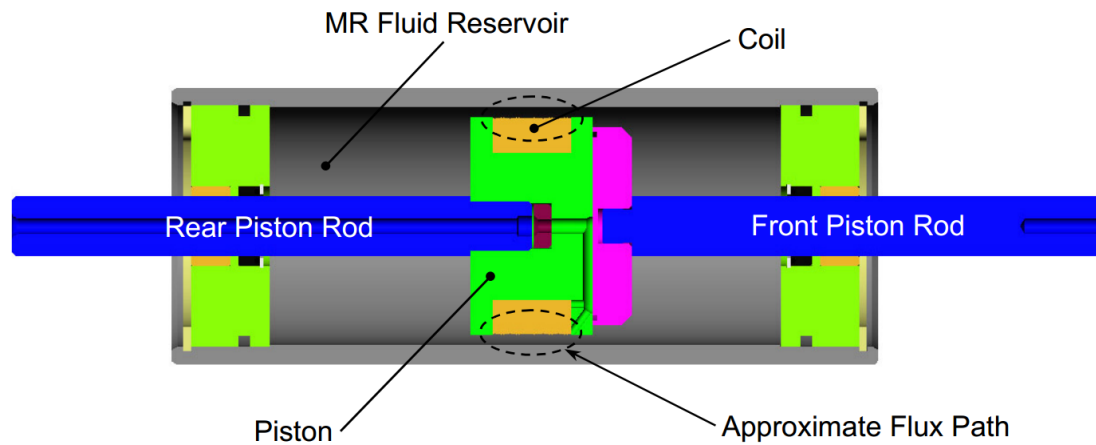

Figure 8-15: Schematic configuration of the double-ended MR damper [Poynor, 2001]